

AD-A206 936

DYNAMICS OF EXCITED HIGH-LYING STATES OF H₂ AND D₂

November 1988

AFOSR-TR-89-0474

Final Report

By: Ravinder Kachru and Hanspeter Helm

Prepared for:

AIR FORCE OFFICE OF SCIENTIFIC RESEARCH
Building 410
Bolling Air Force Base
Washington, DC 20332-6448

Attention: Dr. Ralph Kelly
General Physics Division
Directorate of Physics

Contract No. F49620-86-K-0017

SRI Project PYU-2179
MP 88-234

SRI International
333 Ravenswood Avenue
Menlo Park, California 94025-3493
(415) 326-6200
TWX: 910-373-2046
Telex: 334486

AIR FORCE OFFICE OF SCIENTIFIC RESEARCH (AFOSR)
ATTENTION: DR. RALPH KELLY
GENERAL PHYSICS DIVISION
DIRECTORATE OF PHYSICS
BOLLING AIR FORCE BASE
WASHINGTON, DC 20332-6448
CHIEF, TECHNICAL INFORMATION DIVISION

DTIC
ELECTE
APR 24 1989
S E D



089 4 24 175

REPORT DOCUMENTATION PAGE

Form Approved
OMB No. 0704-0188

1a. REPORT SECURITY CLASSIFICATION UNCLASSIFIED		1b. RESTRICTIVE MARKINGS None	
2a. SECURITY CLASSIFICATION AUTHORITY N/A		3. DISTRIBUTION/AVAILABILITY OF REPORT Approved for public release; distribution unlimited.	
2b. DECLASSIFICATION/DOWNGRADING SCHEDULE N/A		4. PERFORMING ORGANIZATION REPORT NUMBER(S) MP 88-234	
4. PERFORMING ORGANIZATION REPORT NUMBER(S) MP 88-234		5. MONITORING ORGANIZATION REPORT NUMBER(S) AFOSR-TR-89-0474	
6a. NAME OF PERFORMING ORGANIZATION SRI International	6b. OFFICE SYMBOL (if applicable)	7a. NAME OF MONITORING ORGANIZATION AFOSR	
6c. ADDRESS (City, State, and ZIP Code) 333 Ravenswood Avenue Menlo Park, CA 94025		7b. ADDRESS (City, State, and ZIP Code) Same as SC	
8a. NAME OF FUNDING/SPONSORING ORGANIZATION Air Force Office of Scientific Research	8b. OFFICE SYMBOL (if applicable) NP	9. PROCUREMENT INSTRUMENT IDENTIFICATION NUMBER F49620-86-K-0017	
8c. ADDRESS (City, State, and ZIP Code) Building 410 Bolling Air Force Base, DC 20332-6448		10. SOURCE OF FUNDING NUMBERS	
		PROGRAM ELEMENT NO. 61102F	TASK NO. A4
		PROJECT NO. 2301	WORK UNIT ACCESSION NO. N/A
11. TITLE (Include Security Classification) DYNAMICS OF EXCITED HIGH LYING STATES OF H ₂ and D ₂			
12. PERSONAL AUTHOR(S) R. Kachru and H. Helm			
13a. TYPE OF REPORT Final	13b. TIME COVERED FROM May 80 to Oct 88	14. DATE OF REPORT (Year, Month, Day) November 1988	15. PAGE COUNT 76
16. SUPPLEMENTARY NOTATION			
17. COSATI CODES		18. SUBJECT TERMS (Continue on reverse if necessary and identify by block number)	
FIELD	GROUP	SUB-GROUP	
2005		H ₂ , D ₂	
2005			
19. ABSTRACT (Continue on reverse if necessary and identify by block number)			
<p>The spectroscopy and dynamics of Rydberg states of molecular hydrogen is important in modeling discharge and electron beam pumped lasers, molecular ion-electron collisions, and the photoionization of molecular hydrogen. Our primary objective was to investigate the excited states of H₂ and D₂ as two prototypes for a systematic study of manifestations of the static and dynamic interactions governing molecular Rydberg states. Our experimental approach employed a stepwise laser excitation scheme. Detection of the charged molecular, atomic fragments and the energy-analyzed electrons enabled us to measure autoionization, ionization, dissociation, and the competition between them. We studied and analyzed the np autoionizing Rydberg states in H₂. We also studied the competition between photoionization and photodissociation from the C¹Π_u H₂ state. In addition, we performed the first study of the onset of field ionization and the forced rotational autoionization of the np Rydberg states. We demonstrated that the ionization process can be described classically. hydrogen, deuterium.</p>			
20. DISTRIBUTION/AVAILABILITY OF ABSTRACT <input checked="" type="checkbox"/> UNCLASSIFIED/UNLIMITED <input type="checkbox"/> SAME AS RPT <input type="checkbox"/> DTIC USERS		21. ABSTRACT SECURITY CLASSIFICATION UNCLASSIFIED	
22a. NAME OF RESPONSIBLE INDIVIDUAL Dr. Ralph E. Kelley		22b. TELEPHONE (Include Area Code) 202/767-4908	22c. OFFICE SYMBOL NP

UNCLASSIFIED

CONTENTS

INTRODUCTION AND SUMMARY 1

RESULTS 3

Autoionizing np Rydberg States of H₂ 3

Competition Between Photoionization and Photodissociation
from the C¹Π_u State of H₂..... 5

Forced Rotational Autoionization..... 6

Field Ionization..... 6

REFERENCE 8

APPENDICES

- A AUTOIONIZING np RYDBERG STATES OF H₂
- B FOUR-PHOTON DISSOCIATION AND IONIZATION OF H₂
- C FORCED ROTATIONAL AUTOIONIZATION OF HIGH-LYING STATES OF H₂
- D FIELD IONIZATION OF HIGH-LYING STATES OF H₂

Accession For	
NTIS GRA&I	<input checked="" type="checkbox"/>
DTIC TAB	<input type="checkbox"/>
Unannounced	<input type="checkbox"/>
Justification	
By _____	
Distribution/	
Availability Codes	
Dist	Avail and/or Special
A-1	



INTRODUCTION AND SUMMARY

Detailed understanding of the spectroscopy and dynamics of H_2 and D_2 Rydberg states is helpful in modeling phenomena as diverse as electron beam pumped lasers, energetic materials, molecular ion-electron collisions, and stellar atmospheres. In addition, because H_2 and D_2 are the simplest diatomic molecules, detailed understanding of the excited-state dynamics, such as competition between autoionization and dissociation, can serve as a starting point for investigations of more complex molecules and molecular ions. Similarly, to understand the effect of external fields that exist in a variety of situations (such as in a plasma, discharges, or stellar atmospheres) on both the static and decay dynamics of molecular states near the ionization limit, we have to understand the behavior of simpler systems such as H_2 and D_2 . Moreover, the relative simplicity of the H_2 system permits theoretical calculations at a level of sophistication not possible in other systems.

During the last three years, we investigated several aspects of the dynamic interaction of the excited electronic states of H_2 , both in field-free regime and in the presence of an external electric field. Our measurements were made possible by the development of a stepwise laser excitation scheme for H_2 at SRI. The stepwise laser excitation scheme enabled the excitation of a large density of H_2 molecules to a wide variety of excited states with a selected vibrational and rotational quantum number. This selectivity has enabled us to (1) measure the total autoionization rates with very high precision, that is, an order of magnitude improvement over the previous measurements;¹ (2) investigate the physical mechanism of field ionization in H_2 ;² and (3) measure the rotational autoionization induced by an external electric field.³ In addition, we investigated the competition between ionization and dissociation in four-photon excitation of H_2 via the B and C states.⁴

We made the first systematic study of the autoionizing Rydberg states near and above the lowest ionization threshold of H_2 . Because of the stepwise laser excitation scheme employed in our experiment, the autoionizing np states appear as symmetric resonances rather than the highly asymmetric Beutler-Fano profiles observed from the direct photoexcitation from the ground state of H_2 . Our experiments show that the $J = 1$ np states are broader than the $J = 3$ np states converging to the same limit, suggesting that the two states autoionize into the ep and ef continua, respectively. Our observations and analysis with a multichannel quantum defect theory (MQDT) of the $J = 1$ states reveal the large perturbations to the np^2 autoionization Rydberg series converging to the $v^+ = 0$,

$N^+ = 2$ limit of H_2^+ , where v^+ and N^+ are the vibrational and rotational states of H_2^+ , respectively, by the low n states converging to the higher vibrational limits of H_2^+ .¹

We have investigated the competition between dissociation and ionization in four-photon excited H_2 . The $C^1\Pi_u$ $v = 0-4$, $J = 1-3$ states are excited by three-photon excitation from the ground state. Absorption of a fourth photon from the same laser leads to either dissociation, i.e., $H + H$ ($n = 3,4$), or ionization, i.e., $H_2^+ + e$. This branching ratio is monitored in photoelectron spectra, taken with a newly developed permanent magnetic 2 steradian spectrometer. The competition between dissociation and ionization shows a pronounced dependence of the symmetry and also rotational quantum numbers of the C -state. We explain this dependence in term of excitation of dissociative H_2 states in the H_2^+ ionization continuum from which both autoionization and dissociation may occur.⁴

We also performed the first systematic study of forced rotational autoionization of excited Rydberg states of H_2 lying below the lowest ionization threshold of H_2^+ , when a small external electric field (≈ 15 V/cm) is applied. We observed rotational autoionization of $n = 22, 23, 24$, and 25 states of the para- H_2 series converging to the $N^+ = 2$ limit of the vibrationless limit of H_2^+ when an electric field is applied. These states lie below the lowest ionization limit of H_2 . Our observations are accounted for by an intuitive classical ionization model that relates the autoionization process to the lowering of the ionization threshold with the applied field.³

Finally, we performed the first comprehensive study of the field ionization threshold of molecular Rydberg states. We found that the $v = 0$ np series of both orthohydrogen and parahydrogen, converging to the lowest rotational states of H_2^+ , with n ranging from 18 to 30, ionize at fields given in $1/16 n_s^4$, with n_s the effective quantum number at the field at which ionization takes place, given by $n_s = n - 0.5$. The ionization process we observed can be described classically.²

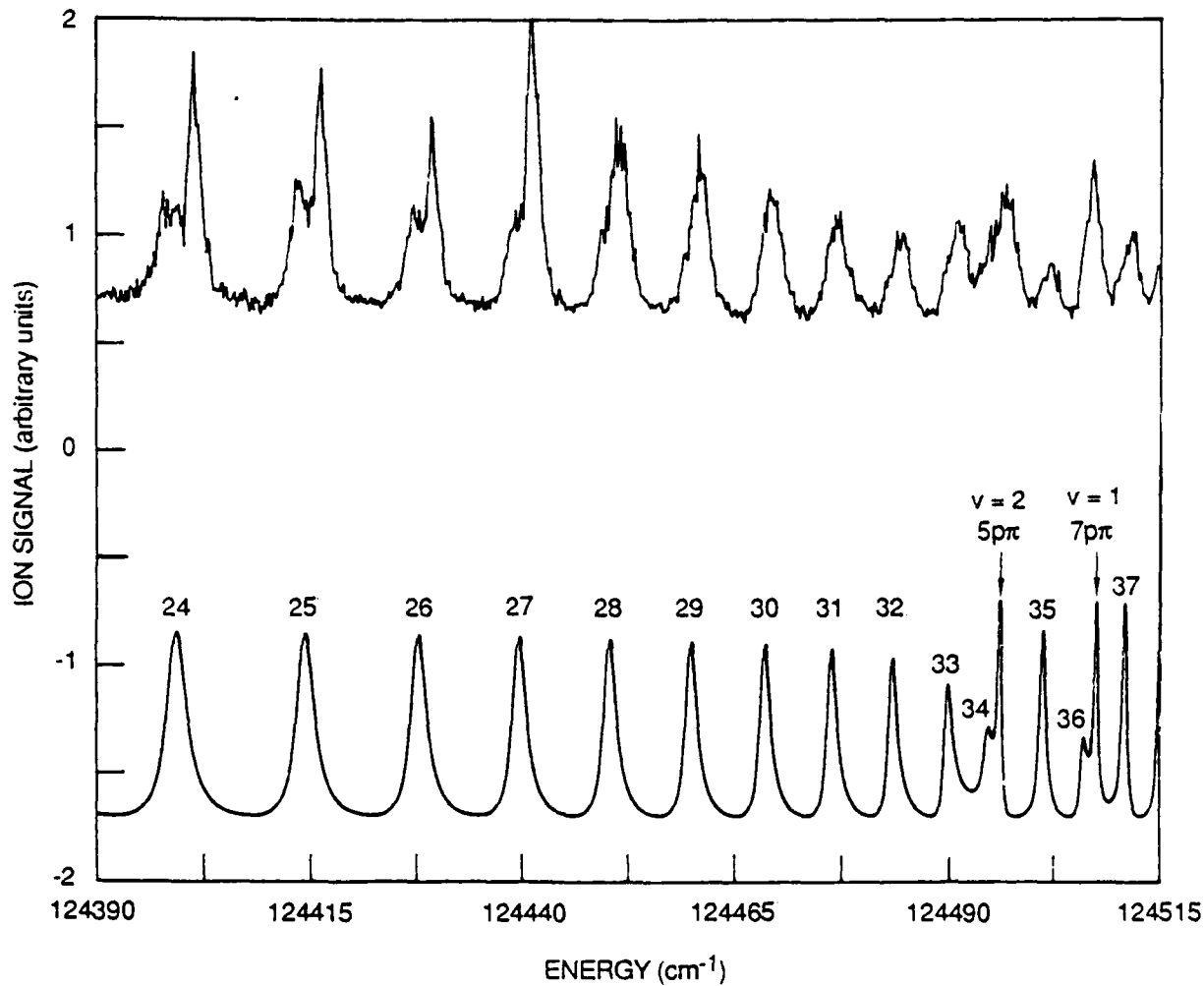
RESULTS

AUTOIONIZING np RYDBERG STATES OF H_2

The study of high-lying excited states of H_2 is important because it is the simplest diatomic molecule and can serve as a prototype for the study of the excited state dynamics for more complex molecules. A strong impetus for the study of H_2 Rydberg states is that, unlike the electrons of helium-like atoms, the Rydberg electron interacts with a nonspherical core having a large quadrupole moment and anisotropic polarizability. This interaction of the Rydberg electron with the molecular core allows dynamic couplings, which lead to rotational and vibrational autoionization.

To the first order, it is expected that the linewidth Γ will scale as n^{-3} . However, as has been shown by the MQDT calculations of Jungen and Dill,⁵ the rotational linewidth is substantially affected in many cases by the vibrational interaction with low n members of Rydberg series converging to high v^+ of the H_2^+ ion. Thus, for analyzing the autoionization spectra, and particularly for analyzing the interactions involved that produce the observed spectra, it is imperative to perform detailed analyses using MQDT, so that the effect of the vibrational autoionization can be delineated from the rotational autoionization. Fortunately, H_2 is one of the few simple systems that allow the use of MQDT with no adjustable parameters to produce synthetic spectra.^{1,5} Thus, accurate measurements of line position, width, and shape will serve as a crucial test for the *ab initio* calculations. We outline below our observation and analysis, which are described in detail in Appendix A.

As a first step toward investigating the effect of rovibrational interaction, we had already performed a preliminary investigation of the $J = 1$ np autoionizing Rydberg states. Figure 1 shows the $J = 1, 2,$ and 3 np Rydberg states excited from the $v' = 0, J' = 2$ E-F state. Each resonance in the top tracing is an np state with two or possibly three J states ($J = 1, 2,$ and 3). The $J = 1$ np state is the low energy part of each resonance. The lower tracing in Figure 1 shows the synthetic spectra obtained from an 8-channel MQDT, folded and depletion broadened. The experimental and MQDT spectra clearly show accurate comparison of theory and experiment. A detailed account of these studies is given in Appendix A.



RA-2179-24B

Figure 1. Experimental and theoretical spectrum.

Excitation spectrum of the autoionizing $v = 0$ np Rydberg states excited from the $v' = 0$ $J' = 2$ E, F intermediate state. The top trace shows the experimental spectrum while the lower trace shows the result of a 8 channel $J = 1$ MQDT calculation. The numbers in the lower trace, indicate the n values of the $J = 1$ $np2$ Rydberg states. The positions of the $J = 1$ $v = 2$ $5p\pi$ state and $v = 1$ $7p\pi$ state are also indicated.

COMPETITION BETWEEN PHOTOIONIZATION AND PHOTODISSOCIATION FROM THE $C^1\Pi_u$ STATE OF H_2

The energy region above the lowest ionization limit of a molecule generally also lies above the lowest dissociation threshold. Excitation of the molecule to this energy regime involves configurations for which two dynamic events, dissociation and ionization, compete. This interplay is illustrated by the dissociative recombination process observed for molecular ions. In the hydrogen molecule, dissociative states that extend into the ionization continuum can be considered as "doubly excited" states or as Rydberg states converging to an electronically excited state of H_2^+ . The lowest of these, $1\sigma_u^2 1\Sigma_g^+$, profoundly affects the excited $1\Sigma_g^+$ states of the neutral molecule and is responsible for the efficient dissociative recombination of the molecular ion.⁶

With the advent of multiphoton excitation experiments, spectroscopic access into this symmetry and this energy domain became possible, and we have carried out an experimental study that probes the interaction between ionization and dissociation channels in the hydrogen molecule.

We observed extensive dissociation in multiphoton excitation via the C-state ($v = 2$) by simultaneously recording the appearance of H^+ and H_2^+ ions. Most striking was the fact that dissociative ionization occurred preferentially on R and P branches, whereas it was significantly smaller when multiphoton excitation occurred in the Q branches. The three-photon excitation wavelengths to the C ($v = 2$) level lie near 2900 Å. At these wavelengths, only the vibrational levels $v^+ > 5$ of H_2^+ are efficiently photodissociated. From the photoelectron spectra of Pratt et al.⁷ it is clear that four-photon ionization via the C state ($v = 2$) does not populate the higher vibrational levels of the ion and hence photodissociation of the parent ion, H_2^+ , could not be the source of the intense photodissociation channel in $v = 2$ excitation. Moreover, the significant difference in the degree of photodissociation associated with populating the C state via the Q or R, P branch could not easily be explained in terms of direct photodissociation of the primary ionization product, H_2^+ .

To assess the nature of the dissociation process, we examined the energy distribution of photoelectrons produced in photoionization of the intermediate $C^1\Pi_u v = 0-4, N = 1-3$ states. The C-state levels are prepared by three-photon single-color resonant excitation in Q and R transitions. Ionization occurs when additional photons are absorbed from the same laser pulse. Our electron spectra show that transitions from the C state can access dissociative electronic states above the ionization threshold from which both dissociation and autoionization may occur. Our findings have triggered a theoretical

treatment of this process.⁸ Our observation and analysis are described in detail in Appendix B.

FORCED ROTATIONAL AUTOIONIZATION

Although in many respects the H_2 Stark states are similar to those for alkali and rare gas atoms, particularly near the field ionization limit, some very important differences unique to molecules lead to somewhat different dynamic behavior for field ionization of H_2 Rydberg states. For instance, in the presence of an electric field, crossing between Stark states of different N and crossing between Stark states associated with different rotational angular moments of the H_2^+ core are avoided.

As an example, consider the np_0 and np_2 states below the lowest $v = 0$ ionization threshold of H_2 . Because $n_0 > n_2$ at any given energy, the np_0 state would be expected to ionize at a field lower than that for the np_2 state. However, owing to the coupling between these two series, an np_2 Rydberg state, because of its mixing with ionizing np_0 levels, will be quenched and start ionizing at a much lower electric field value than it would in the absence of this coupling. Obviously, the extent of the mixing, and hence the dynamics of the ionization process, will depend on the field slew rate.

The considerations of level mixing by the exchange of core rotational angular momentum and the effect of this mixing on the field-induced ionization dynamics apply also to the vibrational mixing. This perturbation leads to mixing of electronic states converging to different vibrational states of H_2^+ . The high v , low n states that are mixed with low v , high n states can field ionize at substantially lower fields. This phenomenon, which has been observed extensively in helium-like alkaline earth atoms, is called forced autoionization. We observed forced rotational autoionization of Rydberg states lying below the lowest ionization threshold of H_2^+ when a small static external field was applied (see Appendix C).³ Similar results were obtained by Janik et al.⁹ in their work on Li_2 . Our observations are accounted for by a classical model.

FIELD IONIZATION

It has long been established that the molecular Rydberg states are field ionizable, and in fact this phenomenon has been employed in many experiments to detect molecules in Rydberg states. Very little except the n^{-4} scaling of the ionization field threshold F_T was known about the ionization process of a molecule in a single quantum state until we performed the first symmetric study of the field ionization threshold of H_2 np Rydberg

states.¹⁰ We found that the $v = 0$ np states of H_2 , with n ranging from 18 to 30 and converging to the $N = 0$ and 1 rotational state of vibrationless H_2^+ core, ionize at fields close to the $1/16 n^4$ classical limit.² For the H_2 np states, like their atomic counterparts, the Coulomb symmetry is broken because of the non-Coulombic potential experienced by the electron in the region close to the core, and, as a result, states of a given n Stark manifold are mixed with states of the adjacent manifold. Another manifestation of the non-Coulombic potential is the non-zero quantum defect of the np states. Appendix D describes in detail how the mixing of the red members of the $N + 1$ Stark manifold with the blue members of the manifold leads to ionization, which can be described classically.

Our experimentally observed threshold field value can be fit into $F_T = 1/16 n_s^4$ where $n_s = n - 0.5$. In the absence of any detailed understanding of the Stark structure of the manifold, we interpret n_s to be the effective quantum number, so that the energy at threshold is $-1/2 n_s^2$. The hydrogenic states, such as high $|m_l|$ states, notably have almost perfect Coulomb symmetry and consequently have no mixing between n manifolds. In such cases, the states dramatically pass from a low to a high field regime and ionize at fields given by $F_T = 1/9 n^4$, which is significantly higher than the value of the classical field observed in our experiments. The details of our field ionization measurements are described in Appendix D.

REFERENCES

1. E. Y. Xu, H. Helm, and R. Kachru (submitted to Phys. Rev. A) (See Appendix A).
2. E. Y. Xu, H. Helm, and R. Kachru, Phys. Rev. Lett. 59, 1096 (1987).
3. E. Y. Xu, H. Helm, and R. Kachru, Phys. Rev. A 38, 1666 (1988).
4. E. Y. Xu, T. Tsuboi, R. Kachru, and H. Helm, Phys. Rev. A 36, 5645 (1987).
5. Ch. Jungen and D. Dill, J. Chem. Phys. 73, 3338 (1980).
6. A. U. Hazi, C. Derkits, and J. N. Bardsley, Phys. Rev. A 27, 1751 (1983).
7. S. T. Pratt, P. M. Dehmer, and J. L. Dehmer, Chem. Phys. Lett. 105, 28 (1984).
8. A. P. Hickman, Phys. Rev. Lett. 59, 1553 (1987).
9. G. R. Janik, D. C. Mullins, C. R. Mahon, and T. F. Gallagher, Phys. Rev. A 35, 2345 (1987).
10. C. F. Barnett, J. A. Ray, and A. Russek, Phys. Rev. A 5, 2110 (1972).

Appendix A

AUTOIONIZING np RYDBERG STATES OF H_2

AUTOIONIZING np RYDBERG STATES OF H_2

E. Y. Xu, H. Helm, and R. Kachru
Molecular Physics Laboratory
SRI International, Menlo Park, CA 94025

ABSTRACT

We report a study of the autoionizing np Rydberg states near the lowest ionization threshold of H_2 . Using resonant two-photon excitation, intermediate states in specific rovibrational levels in the double well, $E,F \ 1\Sigma_g^+$ state are prepared. Then, a second, tunable laser is used to photoionize via excitation of the np Rydberg states. Due to the step wise laser excitation scheme employed in our experiment the photoionization occurs from states with vibrational wavefunctions very similar to those of the H_2^+ core. As a consequence the autoionizing states appear as nearly symmetric resonances, rather than the highly asymmetric Beutler-Fano profiles observed from the direct photoexcitation from the ground state of H_2 . Our experiments show that the $J = 1$ np states are broader than the $J = 3$ np states converging to the same limit, suggesting that the two states autoionize into the ϵ_p and ϵ_f continuum, respectively. We compare our observations with a theoretical analysis using a multi-channel quantum defect theory (MQDT). The $J = 1$ states reveal the profound effect caused by the perturbation of the autoionizing Rydberg series converging to the lowest vibrational and rotational state of H_2^+ by low n states converging to higher vibrational states of the H_2 ion core.

INTRODUCTION

The study of high-lying excited states of H_2 is important because it is the simplest diatomic molecule and can serve as a prototype for the study of the excited state dynamics for more complex molecules. In addition, owing to its relatively simple structure, stringent comparison between theory and experiment is possible. Recently the autoionization of H_2 Rydberg states has attracted considerable attention. For the highly excited states above the ionization limit, autoionization is a leading mechanism of decay. Autoionizing states of molecules are those states for which the sum of the energy of excited electron and the excited core ion exceeds the energy required to ionize the electron. The autoionizing states have inherently short lifetimes and decay by ejecting an electron, leaving the ion in its ground state or in an excited state.

Originally, autoionizing levels were studied using photoexcitation from the ground state with vacuum ultraviolet (vuv) light.¹⁻⁵ Owing to the difference in internuclear separations between the ground state of H_2 and H_2^+ a range of H_2^+ cores are excited with comparable probability from the ground state. As a consequence the excitation line profiles in the threshold region of H_2 appear in the form of complex resonances due to the interference between several bound and continuum channels. The np Rydberg states, excited directly from the H_2 $1\Sigma_g^+$ ground state by the absorption of vuv light were first studied systematically by Herzberg and Jungen² and Takezawa³ in H_2 and D_2 , respectively. These states were monitored by observing the absorption as a function of wavelength through a spectrometer. The autoionizing np states were later studied in greater detail by Dehmer and Chupka,⁵ using the single photon vuv excitation from the ground state, but using H_2^+ ion detection to increase the sensitivity and resolution.

In the present work the autoionizing np states are reached step-wise via a bound intermediate state with vibrational wavefunctions very similar to selected H_2^+ cores. As a consequence nearly symmetric Lorentzian excitation line profiles are obtained for many of the autoionizing states. This is because in the stepwise laser excitation schemes, the excitation cross section to a single autoionization channel can be selectively enhanced. For example, the cross section for excitation of the continuum can be selected to be much smaller than the excitation cross section to the bound part, or the other way around.

Before we describe our present measurements in detail, let us digress briefly on the specific system under study, the H_2 np ($J = 1, 2,$ and 3) states converging to the various rovibrational levels of $X^2\Sigma_g^+ H_2^+$ (see Figure 1). We first excite to either the $v' = 0, 1,$ and 2 vibrational levels of the E,F $1\Sigma_g^+$ ⁸⁻⁹ state from the ground H_2 state with a tunable vuv light using two-photon excitation.¹⁰⁻¹⁴ Using the Q(0) and Q(2) transitions, respectively, we populate the $J' = 0$ and $J' = 2$ rotational levels of parahydrogen in the E,F state. A second dye laser then excites the np Rydberg series from the E-F intermediate state.^{6-7,15} Figure 2 shows the threshold region for the $J = 1$ np Rydberg series in detail. Below the ionization limit are the bound np Rydberg series converging to $N^+ = 0, 2$ limits of limit of $H_2^+(v^+ = 0)$ where N^+ and v^+ refer to the rotational and vibration quantum numbers of the ion. Above the lowest ionization limit are the np Rydberg states converging to $N^+ = 2, v^+ = 0$ are degenerate with the continuum $H_2^+(v^+ = 0, N^+ = 0) + E_p$. In addition the $5p\pi$ and $7p\pi$ states converging to the $H_2^+(v^+ = 2, N^+ = 2)$ and $H_2^+(v^+ = 1, N^+ = 2)$ limits,^{2,5} appear in this energy range. The interaction between the nominal bound states and the underlying continuum leads to autoionization. For instance, the $40p$ state converging to the $H_2^+(v^+ = 0, N^+ = 2)$ limit autoionizes because the $40p$ electron exchanges energy with the $H_2^+(v^+ = 0, N^+ = 2)$ core when the electron is near the core. The interaction between the core and the electron results in a deexcitation of the core to its

rotational and vibrationless state i.e., $H_2^+(v^+ = 0, N^+ = 0)$, whereas the electron gains the energy lost by the core, and is ejected out of the molecule.

Using multi-channel quantum defect theory (MQDT) analysis the ionization threshold region of H_2 has been studied extensively.¹⁶⁻¹⁹ Fano²⁰ analyzed the interaction between the series converging to the $N^+ = 0$ and $N^+ = 2$ rotational limits and established the methodology of the quantum defect theory (QDT) treatment of a molecular system. This treatment was used by Herzberg and Jungen² to discuss their spectra. Jungen and Dill then calculated the para- H_2 photoionization spectrum using MQDT involving 20 channels to explain the $J = 1$ absorption spectra of Dehmer and Chupka⁵, with specific emphasis on the complex resonance arising from the interaction of $5p\pi$ and $7p\pi$ states with the $np0$, $np2$ series to $v^+ = 0$.

The position and shape of the autoionizing resonances contain information about the autoionization rate, the quantum defects, and the coupling between the Rydberg series and the continua in an indirect fashion. This is because for a given total angular momentum and parity the autoionizing molecule state is composed of a variety of channels describing different core + electron configurations. This composition is characterized by channel amplitudes that vary with total energy. The appearance of the autoionizing state as a function of total energy is determined by the projection of the initial state wavefunction onto the channel amplitudes by the dipole operator.

We exploit this fact in the following to selectively enhance channel contributions with specific vibrational and rotational quantum numbers. Choosing the $J = 0$ and $J = 2$ rotational levels of the $E,F \ ^1\Sigma_g^+$ state in the vibrational levels $v = 0, 1,$ and 2 as intermediate states we access the $J = 1$ np ionization continuum from six different initial rovibrational wavefunctions. Six different spectra of the very same ionization continuum are acquired. These provide selected views of the spectral composition of the threshold region of H_2 in terms of the different interacting ionic core channels. We have analyzed the np $J = 1$ autoionizing states above the ionization threshold with the MQDT formulation developed by Jungen and Dill¹⁷.

EXPERIMENT

The experimental arrangement consists of a pulsed H₂ beam, which is turned on for $\approx 100 \mu\text{s}$. The hydrogen beam passes between two plates, spaced 0.5 cm apart and is intersected near the center of plates by two counterpropagating tunable dye laser beams that are focused by lenses of 15-cm focal length. The first dye laser beam, with $\lambda_1 = 190\text{-}202$ nm is produced by frequency doubling the output of a tunable dye laser, and then by Raman shifting to the fourth anti-Stokes order in a high pressure H₂ cell (Figure 3). The first dye laser, with a typical energy of 100 $\mu\text{J/pulse}$ and a spectral width of $\approx 1 \text{ cm}^{-1}$, excites the H₂ molecule from a single $v''J''$ level of the X $1\Sigma_g^+$ electronic state to a selected rovibrational level, $v'J'$, in the E,F $1\Sigma_g^+$ excited state. The second dye laser, with $\lambda_2 = 390\text{-}490$ nm, spectral linewidth of 0.75 cm^{-1} , and energy of 100 $\mu\text{J/pulse}$, subsequently excites the molecule from the selected E,F state into the ionization continuum. The two dye lasers are pumped by two YAG lasers that are externally triggered and temporally separated by 80 nanoseconds. Table I lists the excitation steps connecting various states investigated in this work.

The ions created as a result of autoionization are swept out of the interaction region by a small electric field of 15 V/cm. After passing through a small grid in the field plates the ions are accelerated by another grid and focused before entering a 40-cm long flight tube. The detector is a venetian blind electron multiplier. The minimum DC field applied to the field plates removes the group of ions formed as a result of 2+1 resonant photoionization from the first laser, and thus temporally separates them from the group of ions produced by the absorption of the second laser. The flight tube also temporally separates the H⁺ and H₂⁺ ions. At high backing pressures H₃⁺ ions were also observed. The signal detected by the electron multiplier is amplified and recorded by boxcars and stored in

a PDP-11 computer which also scans the wavelength of the second laser. In order to monitor the frequency of the second laser, we divert a small part of the second laser beam into a 3.313 cm^{-1} free-spectral range etalon and record the intensity of the zero order fringe.

OBSERVATIONS

We have investigated the autoionizing np Rydberg states via different excitation paths emanating from different rovibrational levels of the $E, F \ 1\Sigma_g^+$ state. The E-F intermediate states are excited from $X^1\Sigma_g^+ \ v'' = 0, J'' = 0$ or 2 via the two photon processes listed in Table 1. The inner part of the E-F state can be described as adding a $2s\sigma_g$ Rydberg orbital to the H_2^+ ion core. Thus the inner part of the potential energy curve which we refer to for simplicity as the E-state, can be approximated as a $2s\sigma_g \ 1\Sigma_g^+$ state. That this picture is valid is evidenced by the fact that the equilibrium separation of the E-state, $R_e(E) = 1.011 \text{ \AA}$, is close to that of the H_2^+ ground state, $R_e(H_2^+ \ 2\Sigma_g^+) = 1.06 \text{ \AA}$.⁸⁻⁹

In general, there are three H_2^+ ion core rotational states $N^+ = J-1, J,$ and $J + 1,$ which, when coupled to the $\ell = 1$ Rydberg electron will give an np state with the total angular momentum J . Thus, for instance, starting from a $J' = 0$ E-state, the $J=1$ np Rydberg states converging to the $N = 0$ and $2,$ limits of the H_2^+ core can be excited. On the other hand, starting from the $J' = 2,$ E-state the dipole selection allows the excitation of the two $J = 1$ np states converging to the $N^+ = 0$ and 2 limits, one $J = 2$ np state converging to the $N^+ = 2$ and two $J = 3$ np states converging to the $N^+ = 2$ and $N^+ = 4$ limits, respectively.

Excitation via $v' = 0, J' = 0$

Figure 4 shows the $J = 1$ ionization spectrum as it appears when excited from the $v' = 0, J' = 0$ level of the E state. In this case the dipole selection rule allows the excitation of a single $J = 1$ np series converging to $N^+ = 2$ H_2^+ limit, $np2,$ and the $J = 1$ np series converging to $N^+ = 0$ H_2^+ limit, $np0.$ In Figure 4, the $J = 1$ $np2$ resonances converging to the

$v^+ = 0, N^+ = 2$ limit appear as windows in the continuum above the $v^+ = 0, N^+ = 0$ limit. These windows, which are quite symmetric, appear because laser excitation from the rotationless E state favors those electronic final states that have primarily the $N^+ = 0$ ion core character. Thus, laser excitation, at energies greater than $v^+ = 0, N^+ = 0$ H_2^+ limit favors primarily the H_2^+ ($v^+ = 0, N^+ = 0$) + $e(\epsilon, \ell=1)$ open channel, where ϵ is the energy of free electron. However, the interaction of the continuum with the bound $np2$ series results in the effective null transition in the vicinity of $np2$ states. The resonances in the ion signal shown in Figure 4 do not reach zero value due to the finite bandwidth of the second laser and possibly also because several continua may be open due to the existing small dc electric field that is present in the ionization region. The symmetric window resonances indicate that the Fano-q-factor (which is the ratio of discrete excitation versus the continuum excitation probability) is nearly zero.

An interesting aspect of the experimental spectra shown in Figure 4 is the appearance of windows (or resonances) for $n = 24p$ and $25p$, even though these two states lie below the ionization potential of H_2 by 16.3 cm^{-1} and 2.2 cm^{-1} , respectively. The appearance of $n = 24$ and $25p$ is due to the forced rotational autoionization⁷ caused by the 15 V/cm external field. This external field effectively lowers the ionization potential by $\approx 20 \text{ cm}^{-1}$, allowing the autoionization of the unresolved $np0$ Rydbergs. The intensity of the $np0$ series is modulated by the $n = 24$ and $n = 25$ members of the $np2$ series which appear as windows.

Excitation via $v' = 0, J' = 2$

A drastically different ionization spectrum is obtained when the $v' = 0, J' = 2$ level of the E state is chosen as intermediate. When the second laser is scanned in a frequency range such that the total excitation energy is above the $v^+ = 0, N^+ = 0$ ionization limit at $124417.53 \text{ cm}^{-1}$, we observe sharp resonances corresponding to the Rydberg series

converging to the $v^+ = 0$ $N^+ = 2$ limit at $124591.77 \text{ cm}^{-1}$. The top trace in Figure 5 shows the experimental spectrum. The first two resonances on the low energy side of Figure 5 are $n = 24$ and $25p$ states converging to $v^+ = 0$, $N^+ = 2$ limit, and they appear due to forced rotational autoionization.

Subsequent to a two-photon $Q(2)$ transition from the H_2 ground state $v'' = 0$, $J'' = 2$ to the $v' = 0$, $J' = 2$ E,F state, the dipole selection rule allows the second laser to excite the $J = 1, 2$, or 3 np Rydberg states. Among these the series converging to the $v^+ = 0$, $N^+ = 2$ H_2^+ limit have the highest excitation probability since core rotation is preserved. The electron in the isolated $J = 1$, $np2$ channel is nominally bound but during its close approach to the core can be scattered into the $v^+ = 0$, $N^+ = 0$ ϵp or ϵf open channel leading to ionization.

In examining the ion spectra in the top trace of Figure 5, it is clear that the peaks appear to be split into at least two states. Based on parity considerations, it is possible for $J = 1$ and $J = 3$ states converging to $v^+ = 0$, $N^+ = 2$ H_2^+ limit to autoionize with the ejection of an electron of $\ell = 1$ (p wave) and $\ell = 3$ (f wave), respectively. However, in the absence of an external electric field no such open channel exists for $J = 2$ state, unless the singlet-triplet mixing is significant. The $J = 2$ states may, however, autoionize in the small electric field ($\approx 15 \text{ V/cm}^{-1}$) because of the mixing of ϵp and ϵd continua.

The experimental spectra shown in Figure 5, show that the split resonances have a broad peak at low energy side and a fairly sharp peak at the higher energy side. Some of the widths have been measured with the bandwidth of the second dye laser reduced by an intracavity etalon. For example, at $n = 24$, the broad peak has a width of 0.6 cm^{-1} while the sharp peak has $< 0.3 \text{ cm}^{-1}$ width. At low n the splittings are measurable but at $n \approx 30$ the splittings are smaller than the resolution obtained in our experiment. The separation between the broad and sharp peaks is 3 cm^{-1} at $n = 24$ and decreases with n . When we plot this splitting in cm^{-1} versus n on a log-log scale we observe that the

dependence of this splitting as a function of n is close to n^{-3} . This convinces us that the broad and sharp autoionizing peaks belong to parallel Rydberg series of different J which converge to the same N^+ limit of H_2^+ .

In comparing the position of $J = 1$ spectra of Figure 4 with the spectra in Figure 5, it is clear that the broad part of the resonances for each n , matches with the $J = 1$ window resonances of Figure 4. Thus we attribute the broad part of resonances in Figure 5 to the $J = 1$ state and the sharper resonances to $J = 3$. This interpretation is corroborated by the observation that the $J = 1$ and $J = 3$ autoionize by ejection of p and f electron, respectively. Since the probability of an f electron being near the core is considerably smaller than for p electron, we expect the $J = 3$ rotational autoionization linewidth to be much narrower than that for the $J = 1$ state.

The Rydberg state progressions in Figure 4 and 5 appear fairly regular from the low energy side up to 124490 cm^{-1} , corresponding to $24 \leq n \leq 32$. Beyond 124490 cm^{-1} it is evident that the Rydberg-like progression is disturbed. The perturbing states are the well known¹⁷ $J = 1 \ 7p\pi$ level converging to $v^+ = 1$, and the $5p\pi$ level converging to the $v^+ = 2$ limit of H_2^+ . These are investigated in more detail below.

Excitation via $v' = 1$

The low n states converging to high v^+ of H_2^+ perturb the $J = 1$ series and significantly affect the autoionization process. Two important low n states, also referred to as interlopers in this energy range, are the $7p\pi$ state converging to $v^+ = 1$ limit at $124507.23 \text{ cm}^{-1}$ and the $5p\pi$ state converging to $v^+ = 2$ limit at 124495.5 cm^{-1} . These two states were first observed and assigned by Herzberg and Jungen² and later observed in greater detail by Dehmer and Chupka.⁵

In order to investigate the effect of the $J = 1$ perturbors we have excited the np Rydberg states above the ionization potential starting from the $v' = 1$ E-F state. The top trace in Figure 6 shows the autoionization spectra obtained when the second dye laser excites the np Rydberg states starting from the $v' = 1, J' = 0$ E-F state, as the dye laser is scanned. An important difference between the experimental spectra of Figure 6 and the one shown in Figures 4 and 5, is that the perturber states are now much larger in amplitude because the Franck-Condon factors favor primarily the final states with $v = 1$ character and to a lesser extent the $v = 2$ character. The progression of Rydberg np states shown in Figure 6 consists of a single $J = 1$ series. Each np state consists of a broad resonance, which is consistent with its $J = 1$ character, and with the $J = 1$ spectra of Figure 4.

It is important to note that the observed ion intensity is not proportional to the excitation cross section in Figure 6. In Figure 7, the solid trace shows a part of the observed spectra that is also shown in the top trace in Figure 6. In obtaining the solid trace in Figure 6, the second dye laser has an energy of 1 mJ/pulse. When the dye laser power is reduced by a factor one hundred, i.e., the second dye laser has an energy of 10 μ J/pulse, the spectra shown as dotted line in Figure 7 is obtained. Note that although the intensity of the two main peaks, $v = 2,5p\pi$ and $v = 1,7p\pi$ is roughly the same for the two traces, the width of the peaks at low laser power is significantly smaller and the smaller peaks representing $np2$ resonances appearing at high laser power are missing at lower laser power. When we reduce the laser power below 10 μ J, the width of the autoionizing states does not decrease, suggesting that at very low laser power levels the autoionization width is limited by the laser linewidth. The observations we have shown in Figure 7, in fact apply to all the spectra we present in this paper.

The apparent broadening of the resonances as a function of laser power is well known, and has been termed as depletion broadening,²² because the initial state (in our case the E,F state) is depleted at high laser powers. As will be shown in Section III the

observed ionization signal is proportional to the optical cross section only in the limit $\sigma\phi \ll 1$, where σ is the optical cross section and ϕ the light flux. Thus it may seem sensible to record the entire autoionization spectra at low laser flux. However, we have not done so because, as Figure 7 shows, we would be unable to record the smaller np^2 resonances which have an optical cross section that is smaller by two orders of magnitude than the $5p\pi$ and $7p\pi$ perturber resonances.

Figure 8 shows the ion spectrum when the intermediate state is $v' = 1, J' = 2$ E state. In examining the experimental spectra in Figure 8, we note that at the low energy side we see some sharp peaks which suggest $J = 3$ np^2 series and broad $J = 1$ peaks with much smaller amplitude. The position of the sharp peaks in Figure 8 also match the position of the sharp peaks in Figure 5. These observations are consistent with the spectra shown in Figure 5. Broader peaks are observed for np^2 states near the perturber resonances. We can interpret this behavior as arising from the mixing of the $7p\pi$ and $5p\pi$ character with the $J = 1$ np^2 states, and the amount of mixing being greater for the np^2 states that lie close to these perturbers.

Excitation via $v' = 2$

We have also examined the energy range above the ionization potential of H_2 , by exciting the Rydberg states from the $v' = 2$ and $J' = 0$ and 2 E states. The top trace in Figure 9 shows the ion spectra when the second dye laser is scanned to excite the H_2 molecules from the $v' = 2, J' = 0$ E intermediate state. As is expected from the small Franck-Condon overlap between the $v' = 2$ E state and the $v = 0$ Rydberg state, no np^2 $J = 1$ Rydberg states are observed. Only the $7p\pi$ and $5p\pi$ states that are Franck-Condon favored are observed. The top trace in Figure 10 shows the ion spectra when the intermediate $v' = 2, J' = 2$ is employed. What is interesting here is that $n = 35$ of np^2

series is observed between $7p\pi$ and $5p\pi$ perturbers and $n = 34$ state sits in the shoulder of $5p\pi$ state.

THEORY

The quantum defect theory (QDT) was first applied to the molecular Rydberg states by Fano.²⁰ Fano treated the interaction of the two np series $np0$ and $np2$ converging to the $v^+ = 0$, $N^+ = 0$ and 2 limits of H_2^+ , respectively. The essence of the quantum defect method is to treat the non-isotropic interaction between the Rydberg electron and the atomic or molecular core in terms of a quantum defect μ which corresponds to a phase shift $\delta = \pi\mu$, so that the electron wavefunction outside the core is a coulomb wavefunction with a phase shift δ . Fano's original idea was extended to multiple channels to fit the atomic spectra by Lu²³ and Lee and Lu.²⁴

Jungen and Atabek¹⁶ and Jungen and Dill¹⁷ have applied the MQDT to the interpretation of the lowest Rydberg states of H_2 and D_2 and the analysis of the rotational-vibrational autoionization of np Rydberg states. This formulation of MQDT treats both the rotational and vibrational autoionization simultaneously. In our analysis we closely follow the MQDT formulation developed by Jungen and Dill¹⁷ and Jungen and Atabek.¹⁶ Since the details of the method may be found in References 16 and 17, we outline the procedure here and highlight the details relevant to the present work.

At short distances r of the electron from the molecular core, the wave function is best described by molecular Hund's case b. The short-range wavefunctions are referred to as closed coupled eigen-channels and depend on Λ , the projection of the total orbital angular momentum on the internuclear axis. When the electron is far from the core, the electron-core interaction is best described by the dissociative channel, which depends on the vibrational and rotational state of the ion. Thus there are two sets of wavefunctions corresponding to two channels that are defined in terms of coordinates except for the radial

distance r (the electron radial wavefunction, will depend on the boundary conditions). The closed coupled channels are

$$|\alpha\rangle = |\Lambda R\rangle \quad (1)$$

where $\alpha = 1, P$, where P is the number of channels and R is the internuclear distance. The decay eigen channels of equal number are denoted by the quantum numbers v^+ and N^+ of the H_2^+ core

$$|i\rangle = |v^+ N^+\rangle \quad (2)$$

The transformation between the dissociative and closed coupled wavefunctions is accomplished by the transformation coefficients

$$\langle \alpha | i \rangle = \langle \Lambda | N^+ \rangle^J \chi_{v^+}^{N^+}(R) \quad (3)$$

where $\langle \Lambda | N^+ \rangle^J$ is the transformation between the Hund's case (b) and (d)¹⁹ and $\chi(R)$ is the wavefunction of the ionic core level considered. To account for the variation of the deviation of the core potential from a pure coulomb field, an R dependent quantum defect is introduced for each Λ state, $\mu_\alpha = \mu_\Lambda(R)$. The multichannel wavefunction can be written as a superposition of $|i\rangle$ eigenchannels as

$$\psi = \sum_i |i\rangle \sum_{i'} \{ f_{v_i}(r) \langle i | c | i' \rangle - g_{v_i}(r) \langle i | s | i' \rangle \} B_{i'} = 0 \quad (4)$$

where f and g are the regular and irregular coulomb wavefunctions,¹⁹ respectively. The absolute energy, E_i , is given by $E_i = I_i - \text{Ryd}/v_i^2$, where Ryd is the Rydberg constant for

H_2 , I_i is the ionization energy for the i^{th} channel and v_i is the effective quantum number for the channel i . $\langle ilcli' \rangle$ is given by

$$\langle ilcli' \rangle = \sum_{\Lambda} \langle N^+ | \Lambda \rangle \langle N^+ v^+ | c_{\Lambda} | N^+ v^+ \rangle \langle \Lambda | N^+ \rangle \quad (5)$$

where,

$$\langle N^+ v^+ | c_{\Lambda} | N^+ v^+ \rangle = \int dR \chi_{v^+}^{N^+}(R) \cos \pi \mu_{\Lambda}(R) \chi_{v^+}^{N^+}(R) \quad (6)$$

with a similar expression for $\langle ilsli' \rangle$, except that $\cos \pi \mu_{\Lambda}(R)$ is replaced by $\sin \pi \mu_{\Lambda}(R)$.

To treat the interaction of the $J = 1$ np series converging to the $v^+ = 0$, $N^+ = 2$ limit, with the $5p\pi$ and $7p\pi$ state as well as the $J = 1$ H_2^+ ($v^+ = 0$, $N^+ = 0$) ep continuum, we have used both six and eight channels in our calculations and these are tabulated in Table II. As is indicated in Table II, channel 1 is open, while the rest of the channels are closed. For the eight channel MQDT calculation, all the channels listed in Table II are employed, whereas for the six channel calculation only the first six channels are used. For closed channels, the energy $E_i = I_i - \frac{Ryd}{v_i^2}$ is negative and hence the boundary condition demands that the wavefunction remain finite as $r \rightarrow \infty$. Thus for all closed channels ($i \geq 2$)

$$\sum_{i'} \{ \sin(\pi v_i) \langle ilcli' \rangle + \cos(\pi v_i) \langle ilsli' \rangle \} B_i = 0 \quad (7)$$

The boundary conditions applied to the open channel yields for all open channels i'

$$\sum_{i'} \{ \sin \pi \tau_{\rho} \langle ilcli' \rangle + \cos(\pi v_i) \langle ilsli' \rangle \} B_i = 0 \quad (8)$$

where τ_{ρ} is the eigen phase shift, and $|\rho\rangle$ is the short range collision eigenchannel. There are as many $|\rho\rangle$ eigenchannels as there are open collision channels $|i\rangle$. In our experiment only channel $i = 1$ is open, as is indicated in Table II. Thus, $\rho = 1$ and therefore explicit

reference to ρ can be removed. By solving the set of homogenous linear equations (7 and 8) for each E we can solve for τ . Once τ is known, B_i can be obtained.

It has been shown in Reference 16 that the photoexcitation oscillator strength can be written as

$$\frac{df}{dE} \Big|_i = \frac{2\hbar\nu}{3} \frac{(2J+1)}{(2J'+1)} \Big| \sum_{\rho} e^{i\pi\tau\rho} \langle i|\rho\rangle \sum_i B_i^{\rho} \quad (9)$$

$$\sum_{\Lambda} \int dR \langle N+|\Lambda\rangle^J \chi_{v^+}^{N^+}(R) d_{\Lambda}(R) \chi_{v'}^{J'}(R), \langle \Lambda|J'\rangle |J|^2$$

where d_{Λ} (d_{σ} and d_{π}) is the dipole matrix element connecting the intermediate Σ state to the closed coupled Σ or Π state. In the first approximation we take d_{σ}/d_{π} , independent of R and equal to 1. Furthermore, since the dipole transition moments d_{Λ} are not known accurately, we have calculated the relative oscillator strengths.

Six-Channel MQDT analysis of rotational and vibrational autoionizing states

The six channels considered in our MQDT analysis of the $J = 1$ np states between the H_2^+ $v^+ = 0, N^+ = 0$ and $v^+ = 0, N^+ = 2$ limits are listed as the first six channels in Table II. It is clear that to treat the interaction of the np0 and np2 series converging to $v^+ = 0$ limit, two channels, channels 1 and 2, listed in Table II are required. Between the $v^+ = 0, N^+ = 0$ and $v^+ = 0, N^+ = 2$ limit, i.e., in the rotational autoionization region, channel 1 is open and channel 2 is closed. However, the presence of the two perturbors $v^+ = 1, 7\pi$

and $v^+ = 2,5\pi$ require an additional four channels in the MQDT formulation. This is our motivation for performing the six channel MQDT calculation.

The first step in our calculation is the evaluation of the matrix elements $\langle ilcli' \rangle$ and $\langle ilslil' \rangle$. The $\mu_\sigma(R)$ and $\mu_\Pi(R)$ were taken from Reference 16 and Reference 17, respectively. The H_2^+ molecular potential $v^+(R)$ used in these calculations was taken from Bishop and Wetmore²⁵ and include the adiabatic corrections. The potential and the quantum defects are interpolated from 0.2 to 10.0 a.u. in a mesh size of 0.01 atomic units (a.u.) after extrapolation to short and long R. The vibrational wavefunctions $\chi_{v^+}^{N^+}$ of H_2^+ were calculated by integrating the Schrödinger equations by Numerov-Cooley method. The matrix elements $\langle ilcli' \rangle$ and $\langle ilslil' \rangle$ were calculated by numerically integrating the overlap of $\chi_{v^+}^{N^+}(R)$ and $\chi_{v^+}^{N^+}(R)$ wavefunctions with $\cos\pi g(R)$ ($\sin\pi\mu_\Lambda(R)$) using Simpson's rule from 0.2 to 10.0 a.u. with a 0.01 a.u. grid size.

The ionization limits of H_2^+ were taken from the work of Herzberg and Jungen. The quantum numbers v_i were calculated using the formula, $E = I_i - Ryd/v_i^2$ ($i = 2, \dots, 5$) where the Rydberg constant $Ryd = 109707.42 \text{ cm}^{-1}$ for H_2 . For any given energy, the set of linear homogenous equations 7 and 8 are solved for a non-trivial solution and a value of the effective phase shift in the open channel is obtained. Once τ is determined, B_i can be obtained and normalized. To calculate the excitation cross section [Equation (9)] or the oscillator strength only the Franck-Condon Factors between the E-F state and the $H_2^+ \ ^1\Sigma_g^+$ state need be calculated. The Franck-Condon factors were calculated by numerically integrating the overlap of the E-F wavefunction and H_2^+ wavefunctions. The E-F wavefunctions were calculated in a manner similar to that for the H_2^+ wavefunctions. The molecular potential for the E-F states was obtained from the work of Kolos and Wolniewics.⁸

Before we discuss the comparison of the synthetic spectra obtained using MQDT, we have to consider the effect of depletion broadening of our experimental spectra (see Section III). In the limit of low laser flux the detected ion signal is proportional to the excitation cross section or the oscillator strength df/dE (see Equation 9). At higher laser flux we have to take into account the "depletion broadening",²² of the spectra. For any laser flux the detected signal may be expressed as

$$I = I_0 (1 - e^{-\sigma\phi}) \quad (10)$$

where I_0 is the number of atoms in the intermediate E state, σ is the optical cross section proportional to df/dE and ϕ is the integrated laser flux. From Equation 10 it is clear that the detected signal I is only proportional to the laser flux in the limit $\sigma\phi \ll 1$. In our experiment, for the large peaks, i.e., peaks corresponding to $7p\pi$ and $5p\pi$ states, the product of $\sigma_m\phi = M$ where σ_m is the maximum of the cross section, is between 10 and 100. Thus only when the flux ϕ has decreased by a factor of 100 is it possible to see the detected signal approach the true excitation cross section. As was discussed in Section III, the signal to noise consideration precluded measurement at lower laser intensity. In order to account for the depletion broadening that exist in our data, we multiply the relative cross section obtained from Equation 9 with the depletion broadening given by Equation 10.

The middle trace in Figure 4, shows the 6 channel MQDT calculation of the excitation spectra obtained when the laser excites the $J = 1$ np Rydberg states from the intermediate $v' = 0$ $J' = 0$ E,F state. The middle trace in Figure 4 has a saturation factor $M = 10$. The agreement between theory and experiment is generally good, except at the highest energy, where the experimental spectra is very noisy and unresolved. Because of the relatively large laser linewidth (0.75 cm^{-1}) the width of the observed resonances is limited by the laser linewidth. In comparing the top and middle traces in Figure 4 it is also

clear that the large laser linewidth is responsible for the unresolved structure in the region between the $7p\pi$ and $5p\pi$ perturbers.

The effect of the interplay between the six decay channels considered in the six channel MQDT calculation are best understood by examining the variation of the coefficients B_i 's, which represent the magnitude of the different decay channels in the wavefunction in the autoionizing region as a function of energy. Figure 11 shows the variation of B_i 's_v calculated from the six channel MQDT ($i = 1\dots 6$) as a function of energy. The decay channels i are labeled in Table II. The top trace in Figure 11 shows the variation of B_1 , which is the H_2^+ ($v^+ = 0, N^+ = 0$) ϵp open channel as a function of energy, above the H_2 ionization limit. In comparing Figure 11 with Figures 4 through 10, it is evident that the amplitude B_1 is normally equal to unity except in the vicinity of the autoionizing states, where it passes through zero, because the effective phase shift of the open channel changes by π radians in the vicinity of resonances. Note that in the vicinity of the $5p\pi$ ($v^+ = 2$) and $7p\pi$ ($v^+ = 1$) resonances, B_1 does not decrease to zero because we have not used a fine enough grid size for our calculation. Another interesting aspect of the top trace shown in Figure 11 is that while the window resonances depicting B_1 are symmetric at the lower energy, corresponding to the $np2$ states from $n = 24$ to $n = 31$, the resonances become markedly asymmetric and broader in the energy range in the vicinity of $v^+ = 2$ $5p\pi$ and $v^+ = 1$ $7p\pi$ resonances. Because there is only one open channel in our problem, the shape of the resonances in the amplitude B_1 of the open channel, mirrors that of the autoionizing resonances.

The profound effect of the $5p\pi$ and $7p\pi$ perturbers is evident from the magnitude of the decay channels representing these states in Figure 11. Specifically, in the vicinity of the two perturbers the wavefunction amplitudes B_5 and B_6 which represent H_2^+ ($v=2, N^+=0$) and H_2^+ ($v^+ = 2, N^+ = 0$) decay channels, respectively, are very large. Furthermore, the amplitudes B_5 and B_6 are not just localized at the vicinity of $5p\pi$ state, but are spread over

50 cm^{-1} . Therefore the $np2$ states, converging to $v^+ = 0, N^+ = 2 H_2^+$ limit with n ranging from 29 to 36 have a significant amount of H_2^+ ($v^+ = 2$) np character. Similarly, as Figure 11 shows, the H_2^+ ($v^+ = 2$) np character is mixed into an even wider range of $np2$ states.

We have also performed 8 channel MQDT calculation, by including the $v^+ = 3, J = 1$ channels. The motivation for performing the 8 channel calculation is that in the energy range of interest there is a $4p\pi$ state converging to $v^+ = 3 H_2^+$ limit at $\approx 124117 \text{ cm}^{-1}$. Although the $v = 3 4p\pi$ state lies below the ionization limit it can still affect the position of the states observed in our experiment. The result of the 8 channel MQDT calculation and a saturation factor $M = 5$ is shown in the bottom trace of Figure 4. In comparing the middle and bottom traces in Figure 4, we see that they look almost identical, except for some very subtle differences in the wings of the perturbers. For instance on the high energy side of the $7p\pi$ resonance ($\approx 124495 \text{ cm}^{-1}$) there is a dip in the 6 channel spectra whereas at the corresponding energy there is a peak in the 8 channel spectra. Unfortunately our experimental spectra does not have a fine resolution to discern between the six and eight channel calculations.

The middle trace in Figures 4-6, 8-10 shows the 6 channel MQDT spectra for the $J = 1$ Rydberg states excited from the $v' = 0 J' = 2 E$ state. The corresponding 8 channel MQDT results are displayed as the lower trace in these figures. In the middle trace we have labelled the n values of the $np2$ states and the position of the perturbing states. In comparing the three traces in Figure 5, there is an overall satisfactory agreement between the experimental data and both 8 channel and 6 channel MQDT. An interesting aspect of the 6 channel and 8 channel MQDT calculation is that although the positions of the $np2$ resonances are the same, the position of the $7p\pi$ and $5p\pi$ resonances are slightly different. In the 8 channel case the perturber positions are shifted by $\approx 1-2 \text{ cm}^{-1}$ with respect to the 6 channel calculation. This is surprising in light of the fact that the $4p\pi$ ($v^+ = 3$) state is $\approx 270 \text{ cm}^{-1}$ from both $7p\pi$ and $5p\pi$ states. In examining the three spectra in Figure 5, it is evident

that there is some disagreement between the shape of observed spectra and MQDT calculation in the neighborhood of the $7p\pi$ and $5p\pi$ perturbers. Similar conclusions result from the examination of the observed spectra and the MQDT synthetic spectra in Figures 6, 8, 9, and 10.

Figure 12 shows the calculated relative oscillator strength for transitions from $v' = 1, J' = 0, E$ state to the $J = 1$ Rydberg states, using the 6 channel MQDT calculation. In Figure 12(a) the large difference in excitation cross section (oscillator strength) to the $np2$ states and the $5p\pi$ and $7p\pi$ perturber states is evident. In figure 12(a) the excitation cross section to the perturber states is off scale. Figure 12(b) shows the excitation cross section to the perturber states. In comparing Figure 12(a) and 12(b), it is clear that the peak excitation cross section to the perturber states is at least two orders of magnitude larger than that for $np2$ states. Figure 12(c) shows in detail the excitation cross section to the $v = 2$ $5p\pi$ state. The spectral narrowness of the $5p\pi$ ($v^+ = 2$) state is directly discernable in Figure 12(c). In absence of "depletion broadening" the $5p\pi$ resonance should appear 0.1 cm^{-1} wide. The middle trace in Figure 6 displays the calculated relative excitation cross section shown in Figure 12 with the depletion broadening taken into account. Comparison of Figure 12(a) and Figure 6 shows that the depletion broadening changes the apparent peak excitation cross section dramatically. As the middle trace in Figure 6 indicates, the peak cross excitation section of the $np2$ and perturber states are about equal. In addition the width of the perturber states in Figure 6 is much larger than those calculated with no depletion broadening.

Another interesting aspect of Figure 12(b) is that the calculated width of the $v = 2$ $5p\pi$ resonance is smaller than the $v = 1$ $7p\pi$ resonances. This result is consistent with the fact that the autoionization rate and therefore the autoionization width is strongly dependent on Δv , where Δv is the difference in the the vibrational quantum number of the autoionizing resonance and the vibrational quantum number of the ion core resulting from

autoionization. Finally, we note that in comparing the experimental and MQDT spectra shown in Figure 6, it is obvious that the calculated spectra correctly mimics the initial decrease and subsequent increase in the peak excitation cross section of the np^2 states as n is increased from 24 to 30.

The detailed disagreement in the lineshapes between the observed and synthetic spectra in the energy range between the two perturbbers in most of our spectra is in part due to the limited resolution of the laser, and due to depletion broadening. In addition, the fine details of the spectra are also sensitive to the magnitude of the quantum defect extrapolation to short and long R . Thus it is obvious that in order to provide a stringent test for the validity of the MQDT calculations we will have to improve both the laser linewidth and the sensitivity and signal/noise of our detection system (to help reduce the problems arising from depletion broadening) in future. However, in spite of lack of fine resolution in our experiment our results show overall agreement between our observation and MQDT calculations. Specifically, the large variation in the appearance of the $5p\pi$ and $7p\pi$ interlopers, when excited from different cores of the E,F state, is correctly reproduced in the MQDT calculations.

CONCLUSION

We have examined the positions and linewidths of autoionization np Rydberg states in the energy range between the $v^+ = 0, N^+ = 0$ and $v^+ = 0, N^+ = 2$ H_2^+ limit. Owing to the stepwise laser excitation scheme used in our experiment, the autoionizing Rydberg states appear as symmetric resonances, instead of the highly asymmetric Beutler-Fano profiles obtained from the direct photoexcitation from the ground state. We have excited the np Rydberg state via several rovibrational E,F intermediate state. As noted previously the $J = 1$ $np2$ Rydberg states are profoundly affected by the presence of low n perturbers, converging to higher vibrational state of H_2^+ . We show that the appearance of the perturbers in the ionization spectrum is strongly influenced by the specific excitation path chosen. We have compared our experimental results with a six and eight channel MQDT calculations. We find that there is a good agreement between theory and experiment. However the comparison between theory and experiment can be more stringent if the linewidth of the laser is reduced and the depletion broadening diminished by improving the signal/noise of the detection system.

ACKNOWLEDGEMENT

Helpful discussions with D. L. Huestis are gratefully acknowledged. This work is supported by the U.S. Air Force Office of Scientific Research under Contract No. F49620-86-K-0017.

REFERENCES

1. G. Herzberg, Phys. Rev. Lett. 23, 1081 (1969).
2. G. Herzberg and Ch. Jungen, J. Mol. Spectrosc. 41, 425 (1972).
3. S. Takezawa, J. Chem. Phys. 52, 2575 (1970).
4. W. A. Chupka and J. Berkowitz, J. Chem. Phys. 51, 4244 (1969).
5. P. M. Dehmer and W. A. Chupka, J. Chem. Phys. 65, 2243 (1976).
6. N. Bjerre, R. Kachru, and H. Helm, Phys. Rev. A 31, 1206 (1985).
7. E. Y. Xu, H. Helm, and R. Kachru, Phys. Rev. A 38, 1666 (1988).
8. W. Kolos and L. Wolniewicz, J. Chem. Phys. 50, 3328 (1969).
9. T. E. Sharp, Atomic Data 2, 119 (1971).
10. D. J. Kligler and C. K. Rhodes, Phys. Rev. Lett. 40, 309 (1978).
11. D. J. Kligler, J. Bokor, and C. K. Rhodes, Phys. Rev. A 21,
607 (1980).
12. H. Pummer, H. Egger, T. S. Luk, T. Srinivasan, and C. K. Rhodes,
Phys. Rev A 28, 795 (1983).
13. E. E. Marinero, C. T. Rettner, and R. N. Zare, Phys. Rev. Lett.
48, 1323 (1982).

14. E. E. Marinero, R. Vasudev, and R. N. Zare, *J. Chem. Phys.* 78, 692 (1983).
15. W. L. Glab and J. P. Hessler, *Phys. Rev. A* 35, 2102 (1987).
16. Ch. Jungen and O. Atabek, *J. Chem. Phys.* 66, 5584 (1977).
17. Ch. Jungen and D. Dill, *J. Chem. Phys.* 73, 3338 (1980).
- 18.. M. Raoult and Ch. Jungen, *J. Chem. Phys.* 74, 3388 (1981).
19. Ning Yi Du and Chris H. Greene, *J. Chem. Phys.* 85, 5430 (1986).
20. U. Fano, *Phys. Rev. A* 2, 353 (1970).
21. E. Y. Xu, H. Helm, and R. Kachru, *Phys. Rev. A* 38, 1666 (1988).
22. W. E. Cooke, S. A. Bhatti, and C. L. Cromer, *Opt. Lett.* 7, 69 (1982).
23. K. T. Lu, *Phys. Rev. A* 4, 579 (1971).
24. C. M. Lee and K. T. Lu, *Phys. Rev. A* 8, 241 (1973).
25. D. M. Bishop and R. W. Wetmore, *Mol. Phys.* 26, 145 (1973).

Table 1. Initial, Intermediate and Final States

Lower State $v'' J''$	Laser 1 λ (nm)	Intermediate State $v' J'$	Laser 2 λ (nm)	Final States $v^+ = 0$
0,0	201.68	0,0	≈ 396	J=1
0,2	202.02	0,2	≈ 399	J=1,2,3
0,0	197.05	1,0	≈ 436	J=1
0,2	197.40	1,2	≈ 439	J=1,2,3
0,0	193.13	2,0	≈ 479	J=1
0,2	193.54	2,2	≈ 482	J=1,2,3

Table 2. MQDT Channels

<u>Channel Number</u>	<u>Decay Channel</u>
1	$ v^+=0 N^+=0\rangle$
2	$ v^+=0 N^+=2\rangle$
3	$ v^+=1 N^+=0\rangle$
4	$ v^+=1 N^+=2\rangle$
5	$ v^+=2 N^+=0\rangle$
6	$ v^+=2 N^+=2\rangle$
7	$ v^+=3 N^+=0\rangle$
8	$ v^+=3 N^+=2\rangle$

FIGURE CAPTIONS

- Figure 1 Potential energy curves for H_2 and H_2^+ and the laser excitation scheme for final ungerade states.
- Figure 2 Details of the np H_2 Rydberg states near the ionization limit. The relevant np Rydberg states converging to various v^+ limits of H_2^+ are labelled by n values. The np_0 and np_2 continua is indicated by columns of slanting lines.
- Figure 3 Schematic of the experimental apparatus.
- Figure 4 Excitation spectrum of the Rydberg autoionizing np ($v^+ = 0$) Rydberg states excited from the $v' = 0, J' = 0$, level of the E,F intermediate state. The top trace shows the experimental spectrum while the center and lower traces show the results of a 6 and 8 channel $J = 1$, MQDT calculation, respectively. The numbers in the middle trace indicate the n values of the ($J = 1$) np_2 Rydberg series. The position of the ($J = 1$), $5p\pi$ ($v^+=2$) and the $7p\pi$ ($v^+=1$) are also labeled.
- Figure 5 Excitation spectrum of the autoionizing np ($v^+ = 0$) Rydberg states excited from the $v' = 0, J' = 2$ level of the E,F intermediate state. The top trace shows the experimental spectrum while the center and lower trace show the results of a 6 and 8 channel $J = 1$, MQDT calculation, respectively. The numbers in the middle trace indicate the n value of

the ($J = 1$) $np2$ Rydberg states. The position of the ($J = 1$) $5p\pi$ ($v^+=2$) and the $7p\pi$ ($v^+=1$) states are also labeled.

Figure 6 Excitation spectrum of the autoionizing np ($v^+ = 0$) Rydberg states excited from the $v' = 1, J' = 0$ level of the E,F intermediate state. The top trace shows the experimental spectrum while the center and lower trace show the results of a 6 and 8 channel, $J = 1$ MQDT calculation, respectively. The numbers in the middle trace indicate the n values of the ($J = 1$) $np2$ Rydberg series. The position of the ($J = 1$) $5p\pi$ ($v^+=2$) and the $7p\pi$ ($v^+=1$) states are also labeled.

Figure 7 The depletion broadening of the autoionization spectrum in the vicinity of the $5p\pi, 7p\pi$ interlopers when excited from the $v' = 1, J' = 0$ level of the E,F intermediate state. The solid trace is a portion of the experimental spectra shown in Figure 6 and recorded with the 1mJ/pulse output of the second dye laser. The broken trace is recorded with the output of the second dye laser set at 10 μ J/pulse.

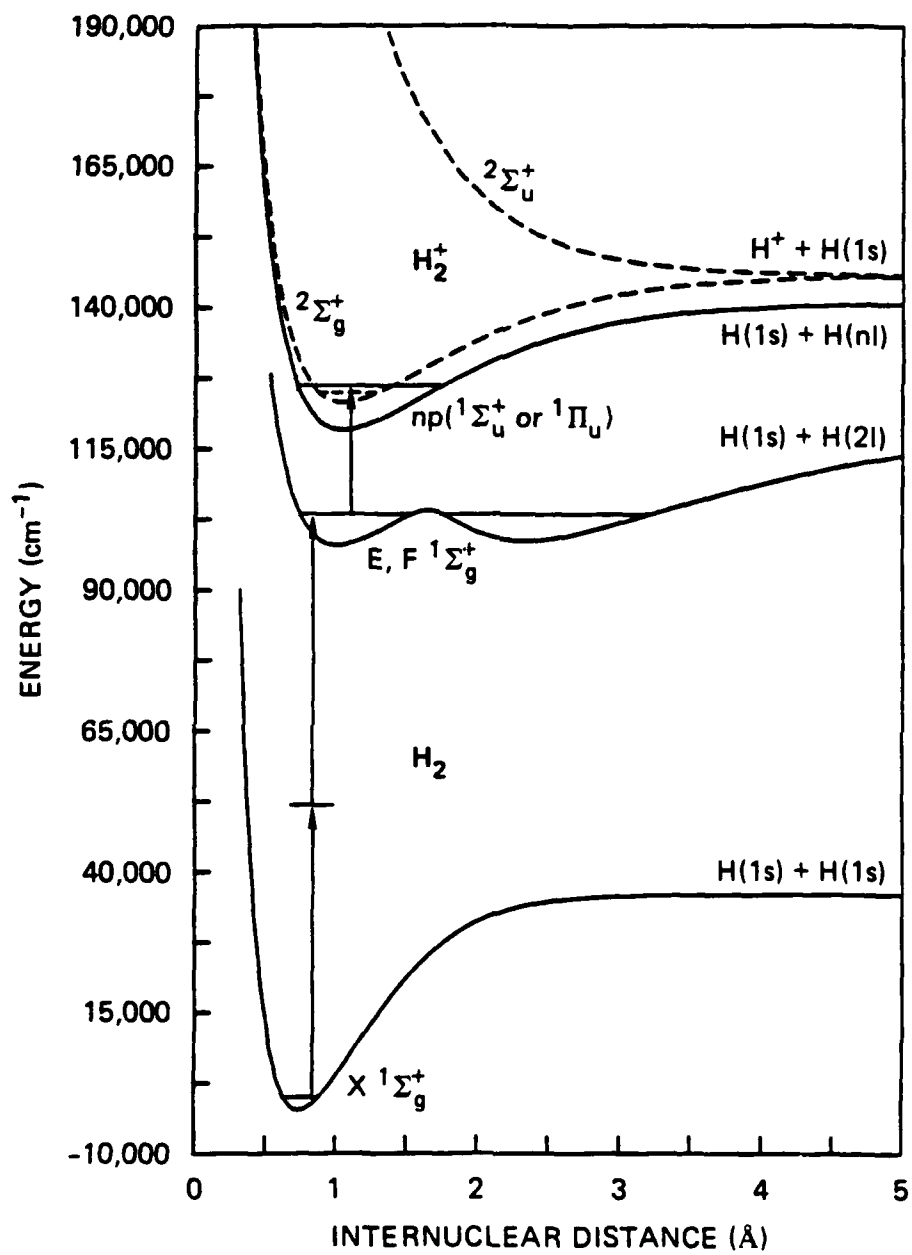
Figure 8 Excitation spectrum of the autoionizing np ($v^+ = 0$) Rydberg states excited from the $v' = 1, J' = 2$ level of the E,F intermediate state. The top trace shows the experimental spectrum while the center and lower trace show the results of a 6 and 8 channel $J = 1$, MQDT calculation, respectively. The numbers in the middle trace indicate the n values of the ($J = 1$) $np2$ Rydberg series. The position of the ($J = 1$) $5p\pi$ ($v^+=2$) and the $7p\pi$ ($v^+=1$) states are also labeled.

Figure 9 Excitation spectrum of the autoionizing np ($v^+ = 0$) Rydberg states excited from the $v' = 2, J' = 0$ level of the E,F intermediate state. The top trace shows the experimental spectrum while the center and lower trace show the results of a 6 and 8 channel $J = 1$, MQDT calculation, respectively.

Figure 10 Excitation spectrum of the autoionizing np ($v^+ = 0$) Rydberg states excited from the $v' = 2, J' = 2$ level of the E,F intermediate state. The top trace shows the experimental spectrum while the center and lower trace show the results of a 6 and 8 channel $J = 1$, MQDT calculation, respectively. The numbers in the middle trace indicate the n values of the ($J = 1$) np^2 Rydberg series. The position of the ($J = 1$) $5p\pi$ ($v^+=2$) and the $7p\pi$ ($v^+=1$) states are also labeled.

Figure 11 Energy dependence of the coefficients B_i ($i = 1,2,\dots,6$) as a function of energy, calculated using a 6 channel MQDT (see text for details).

Figure 12 Excitation spectrum of the $J = 1$ autoionizing Rydberg State excited from the $v' = 1, J' = 0$ level of the E,F intermediate state, calculated with 6 channel MQDT. The depletion broadening is unaccounted for in this spectrum, and is to be contrasted with the spectra displayed in the middle trace of Figure 6 in which the depletion broadening mechanism which is present under our experimental conditions is accounted for.



JA-330532-51C

Figure 1

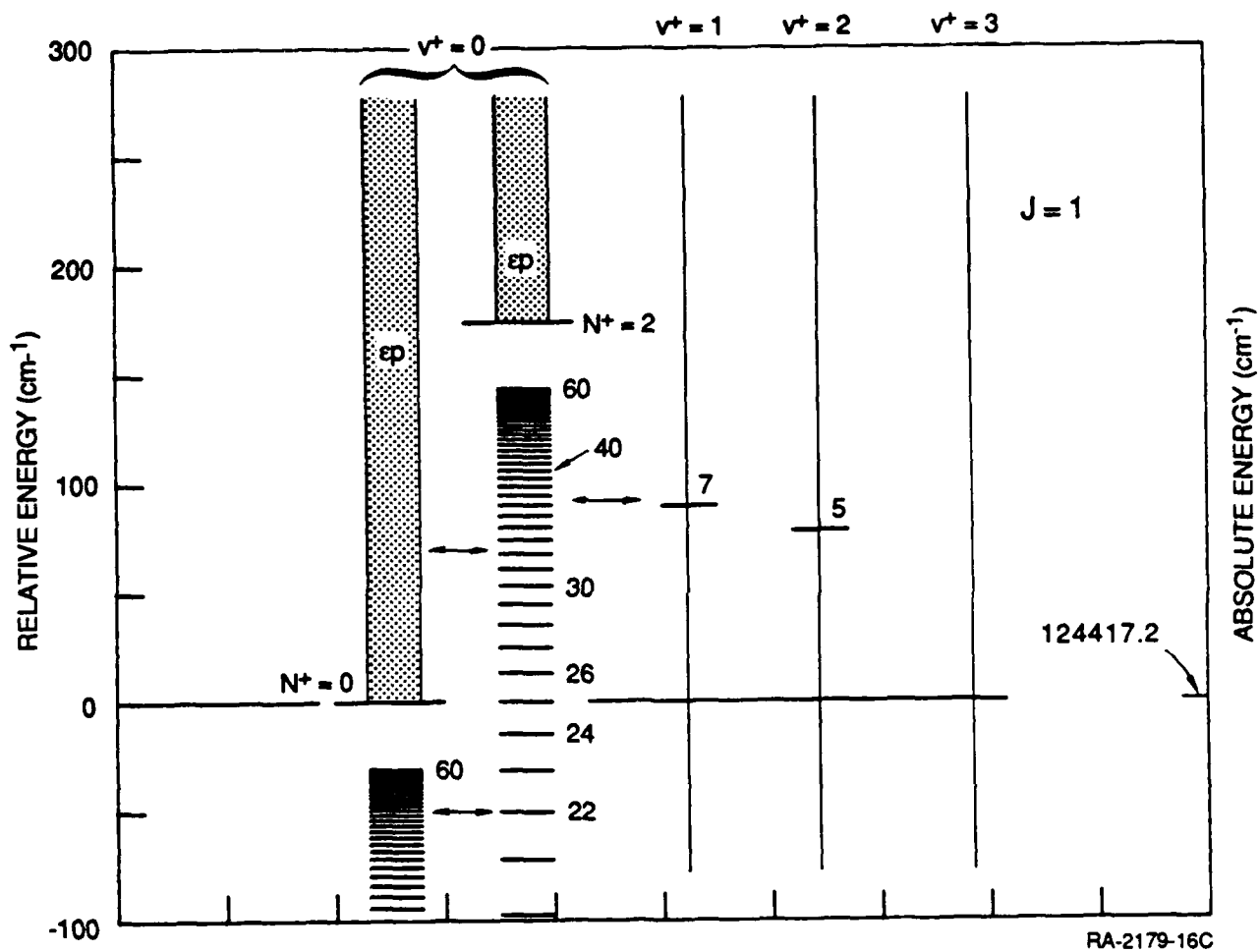
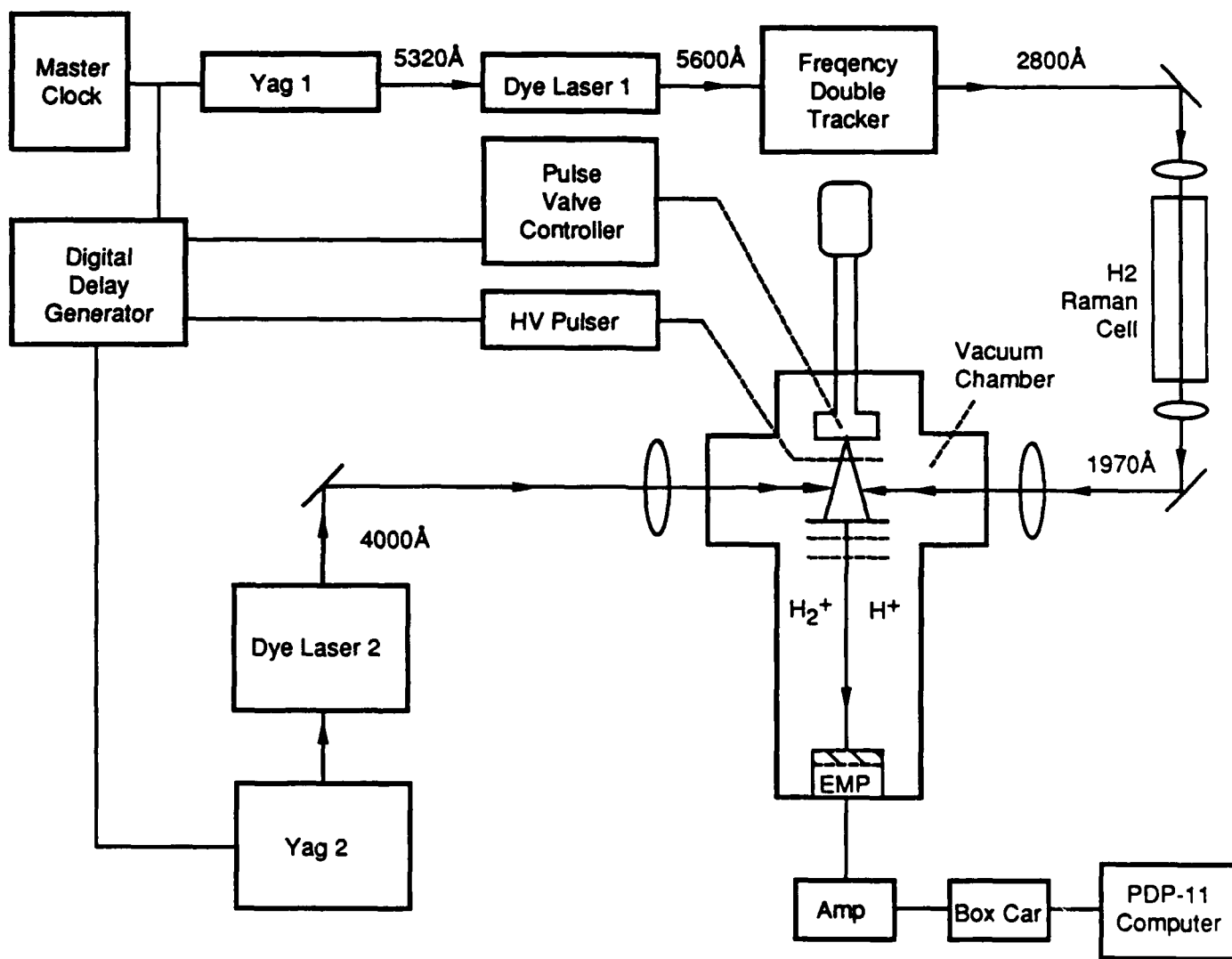
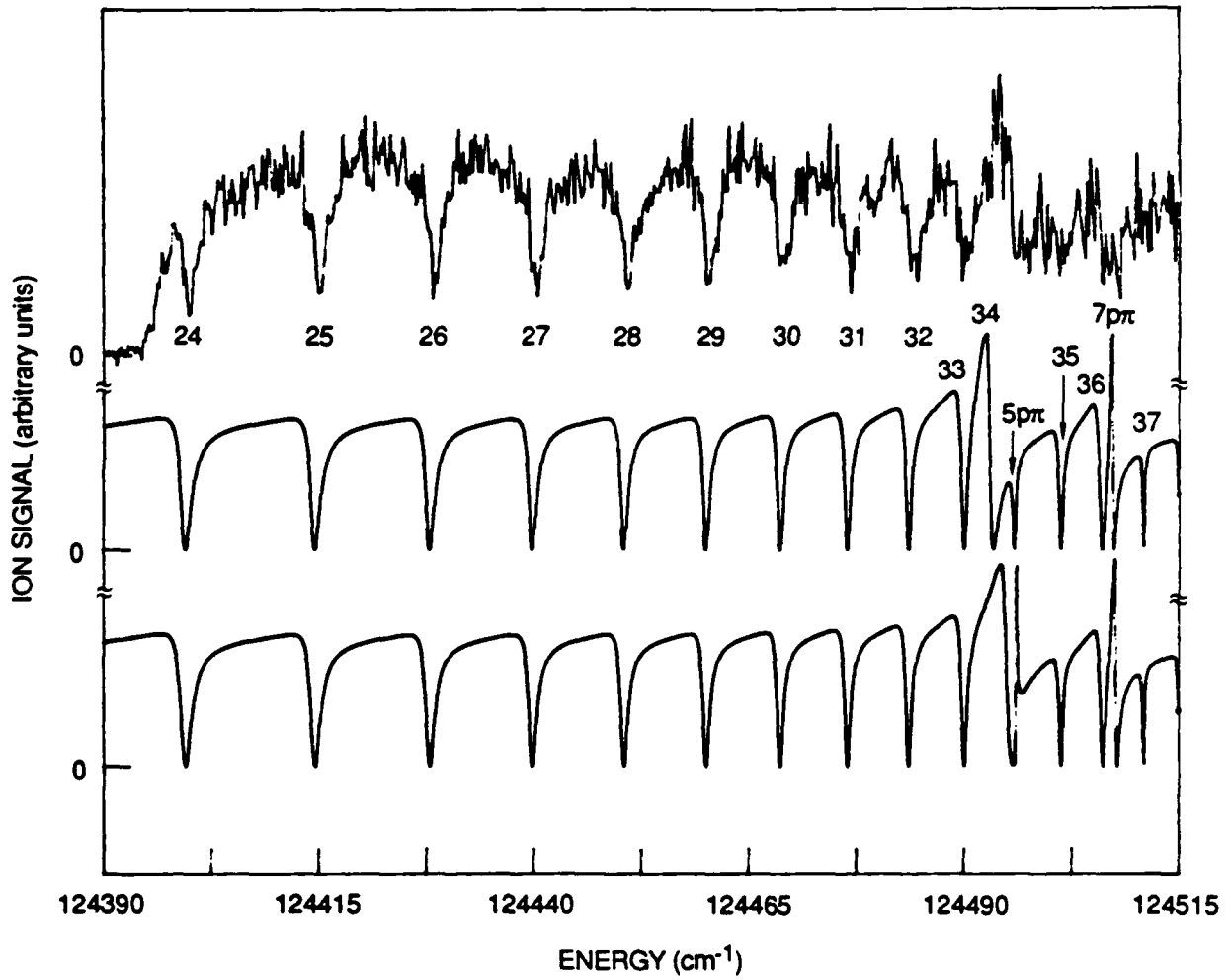


Figure 2



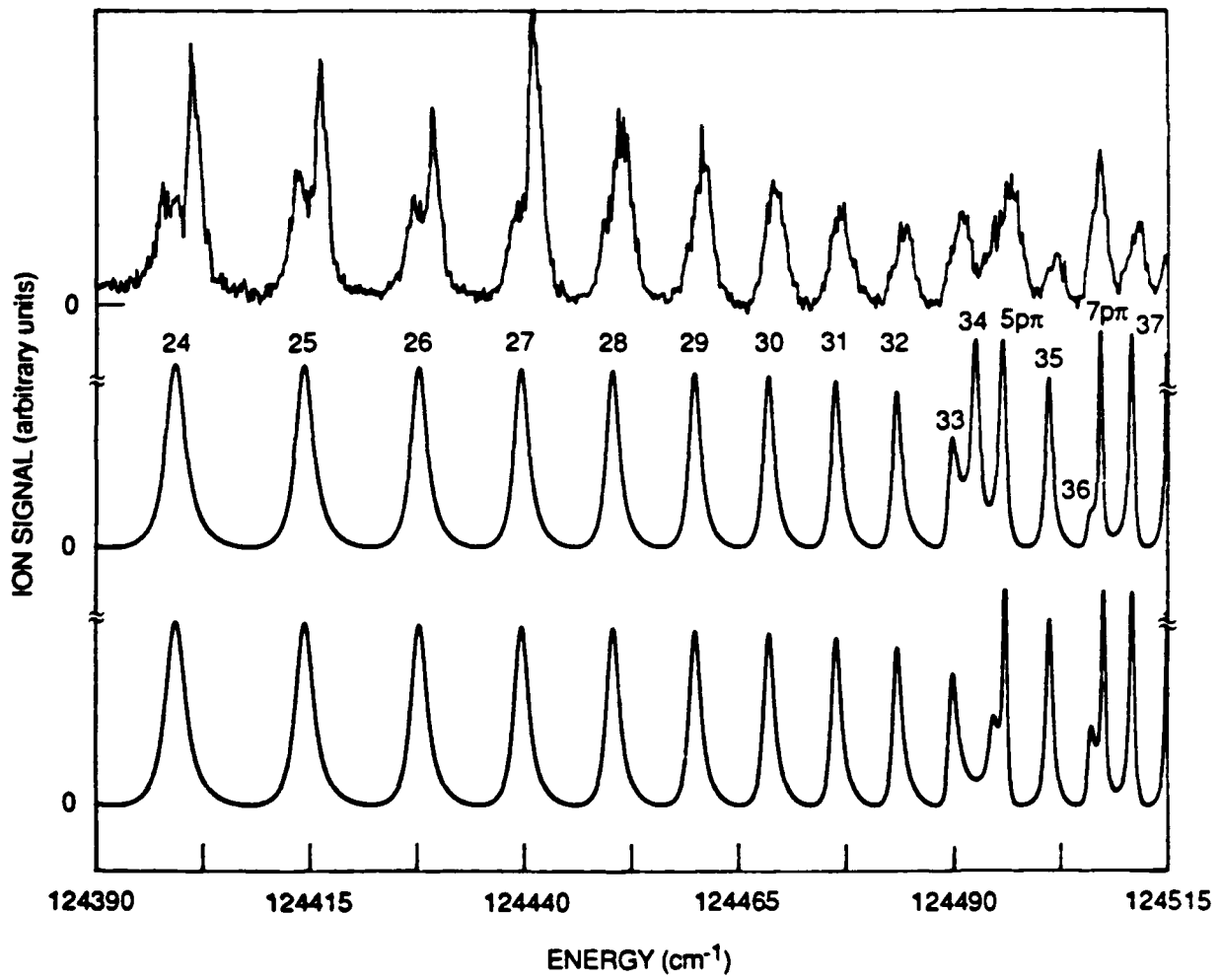
RA-M-2179-28

Figure 3



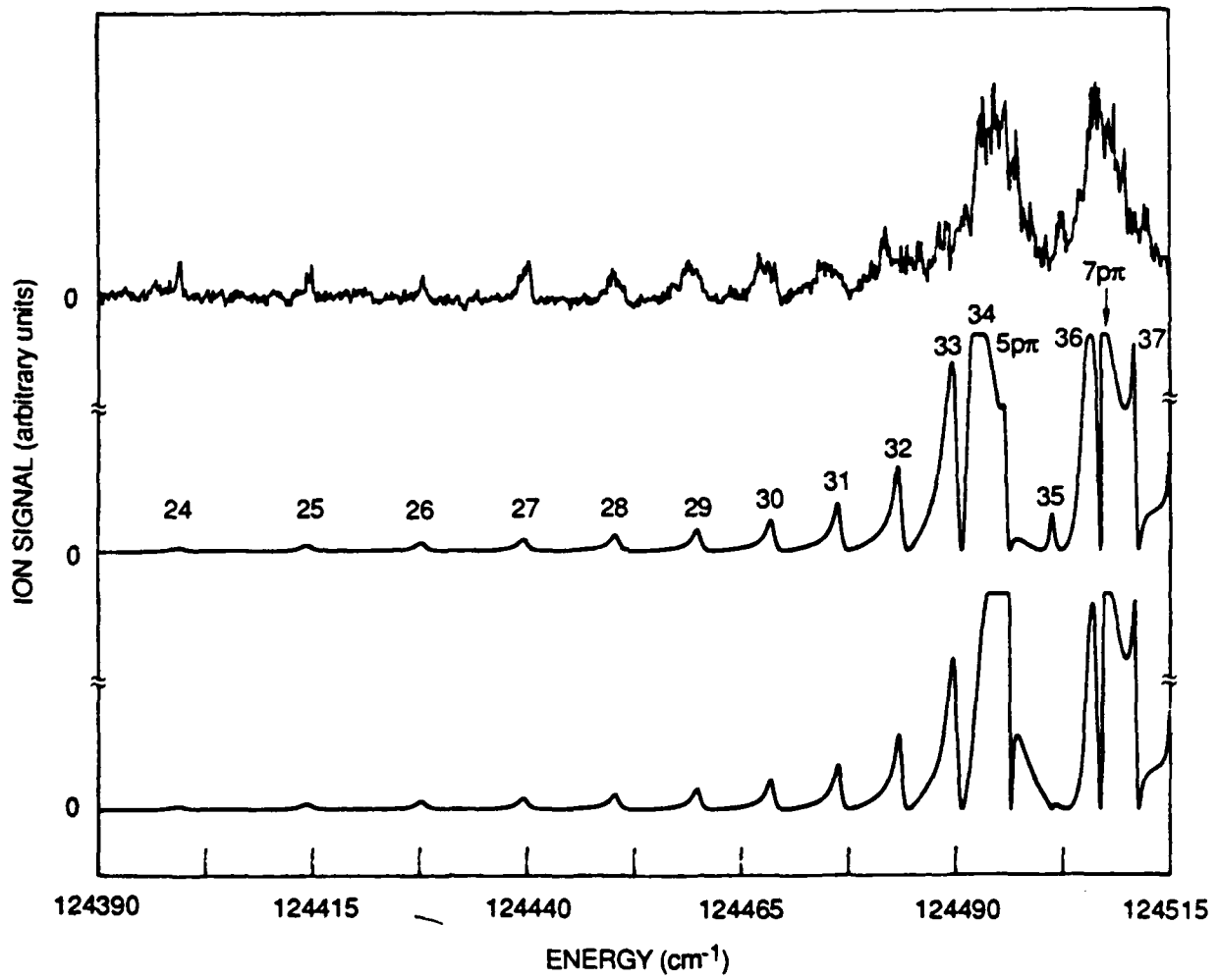
RA-2179-21A

Figure 4



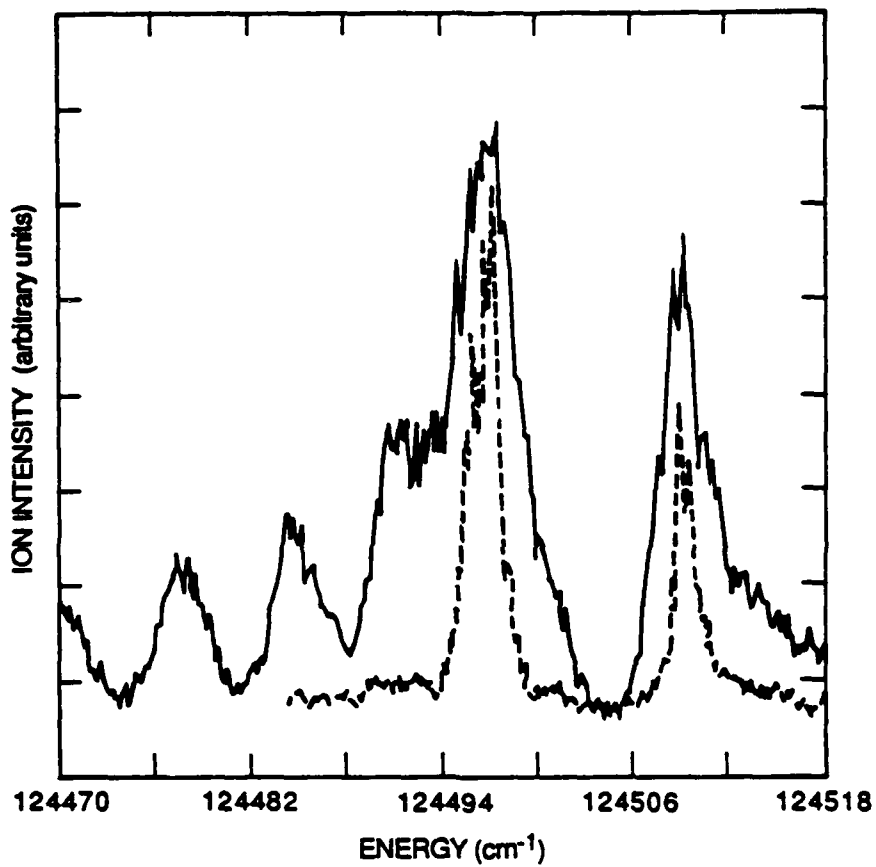
RA-2179-24C

Figure 5



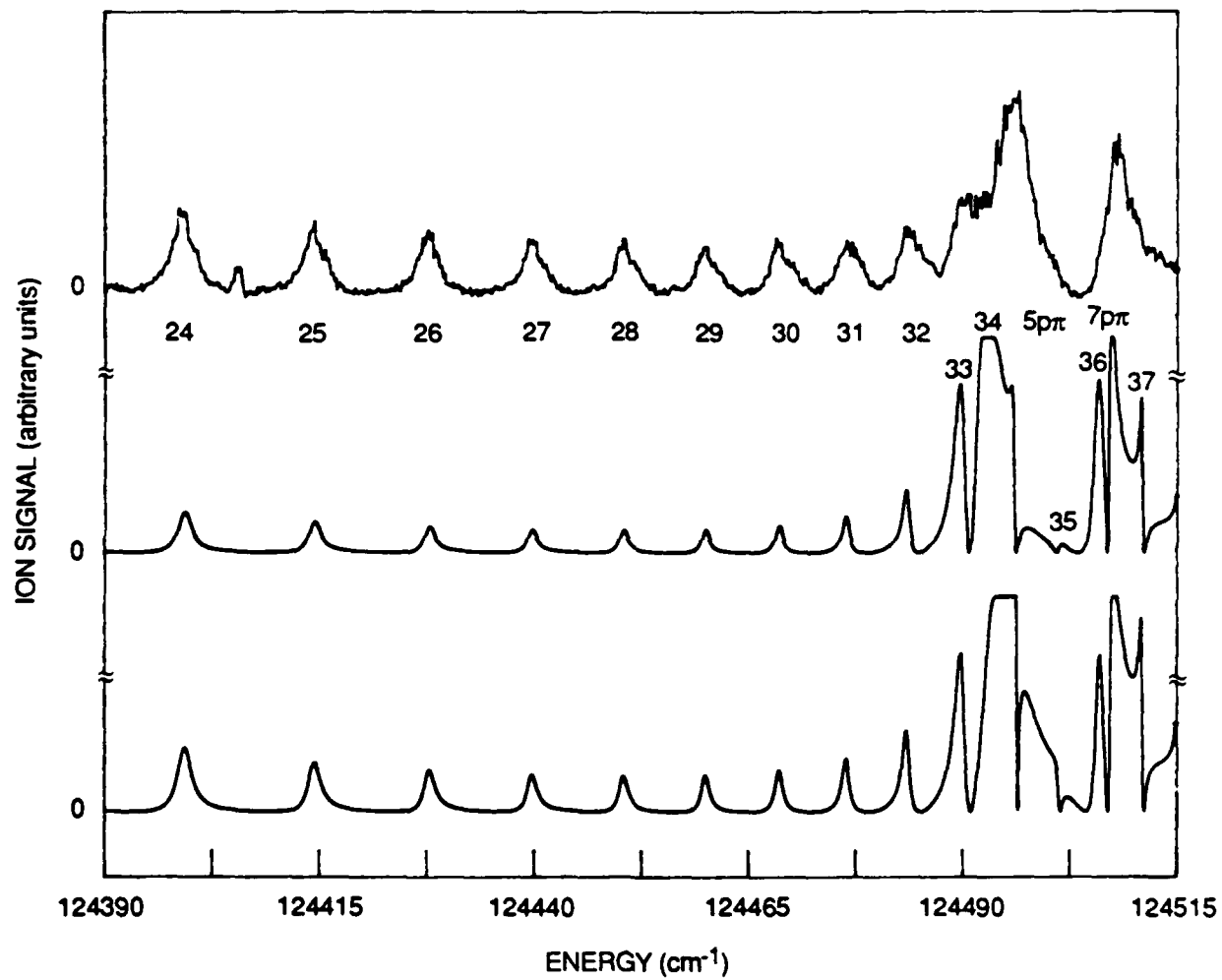
RA-2179-25A

Figure 6



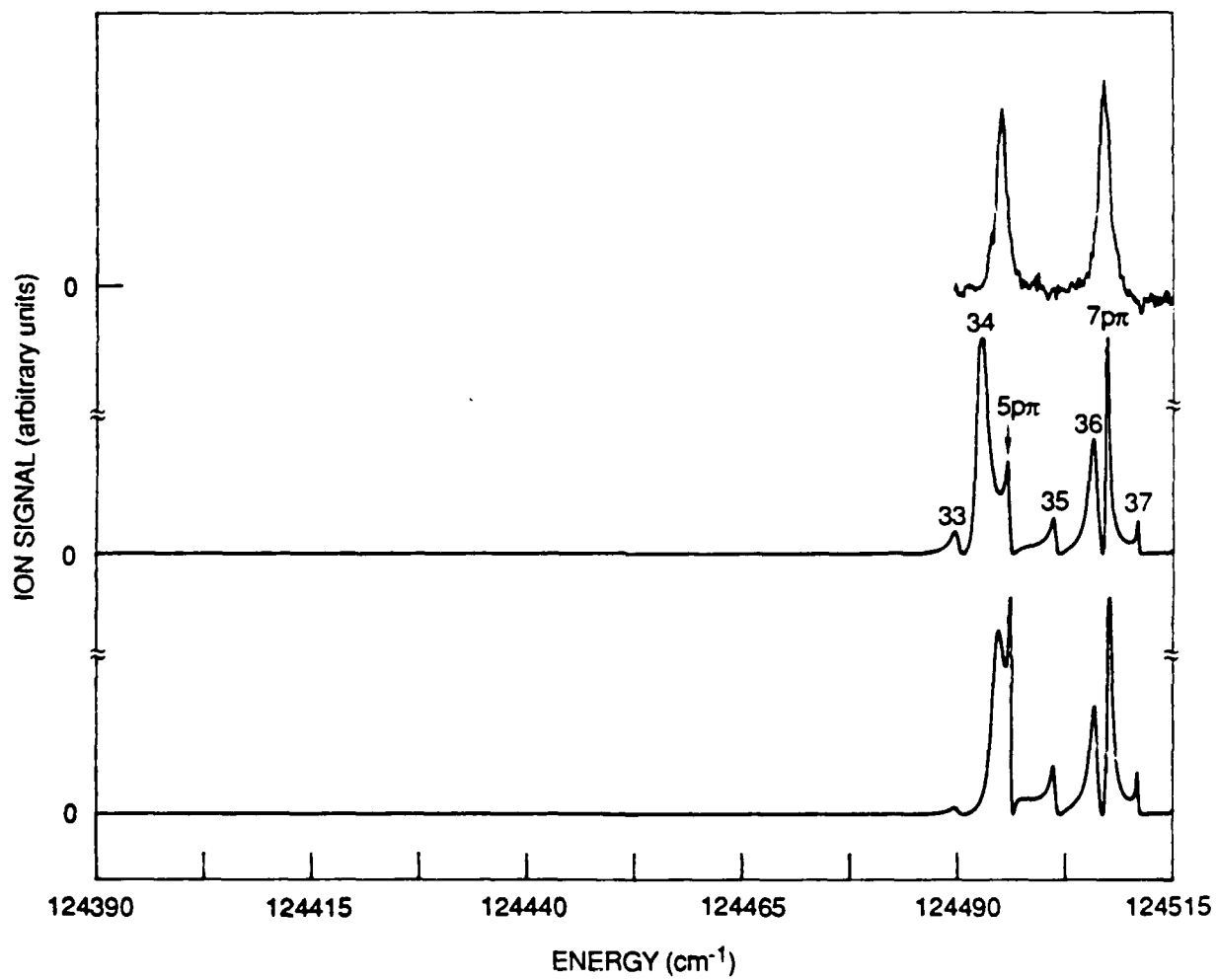
RA-2179-27

Figure 7



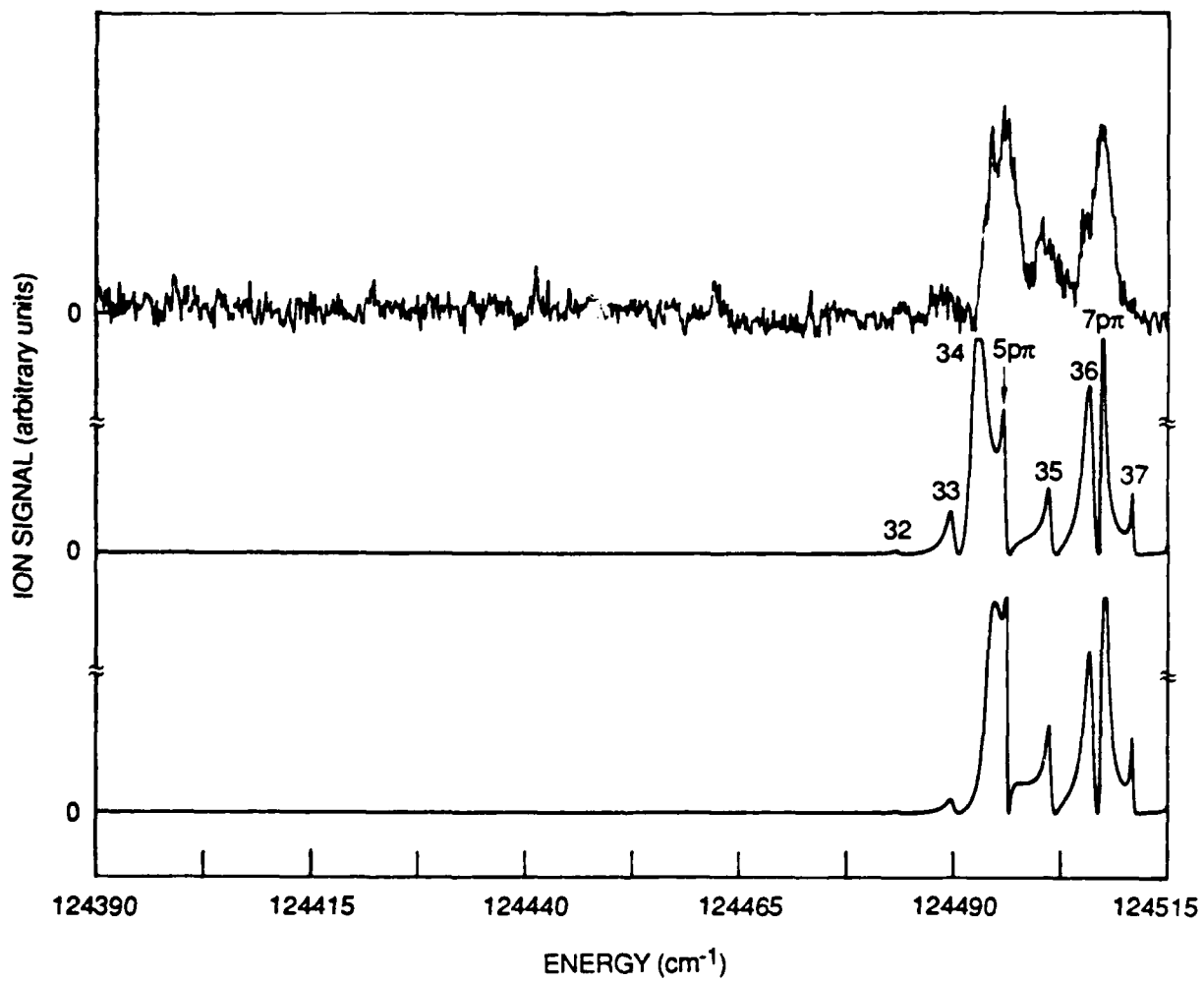
RA-2179-22A

Figure 8



RA-2179-23A

Figure 9



RA-2179-26A

Figure 10

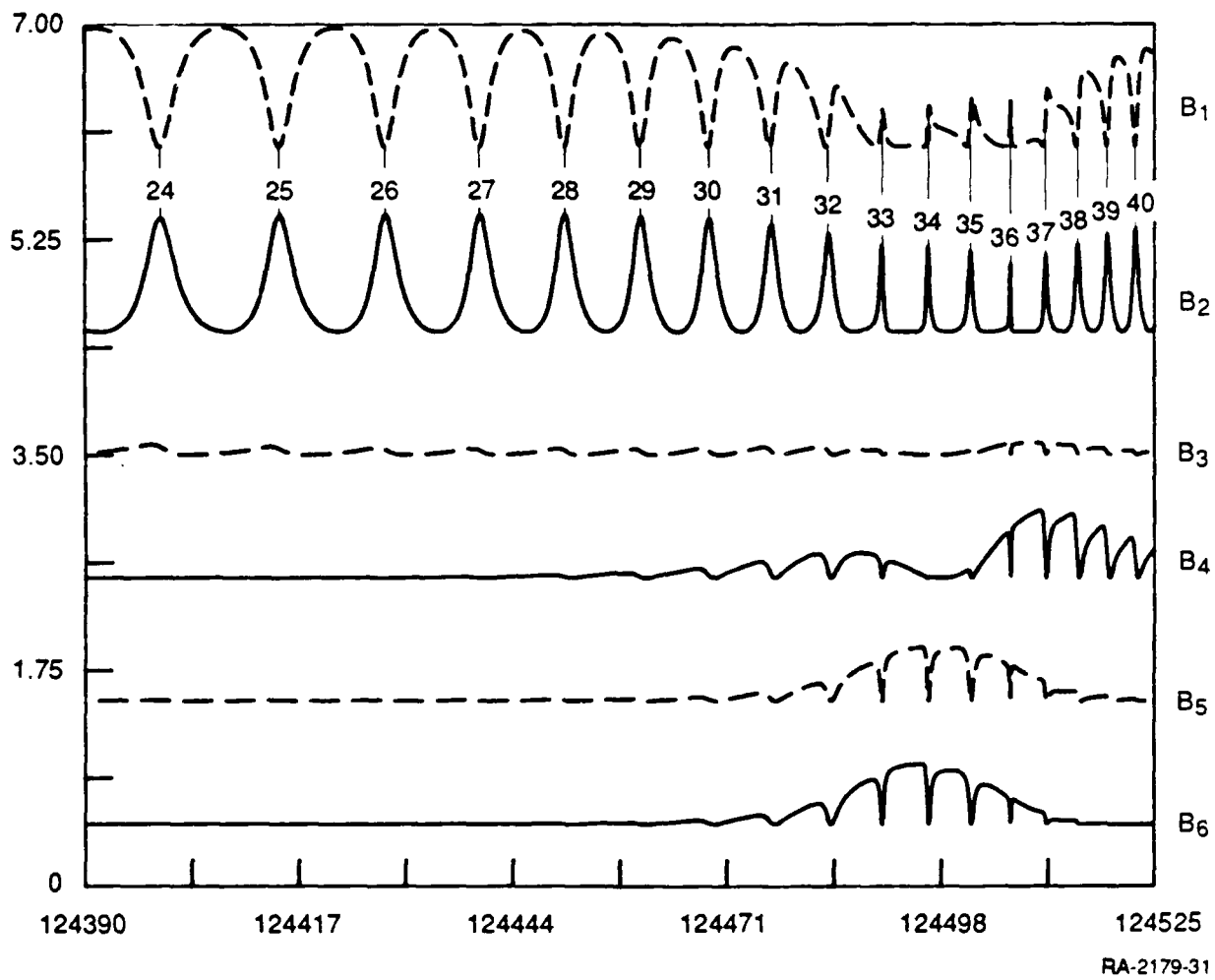


Figure 11

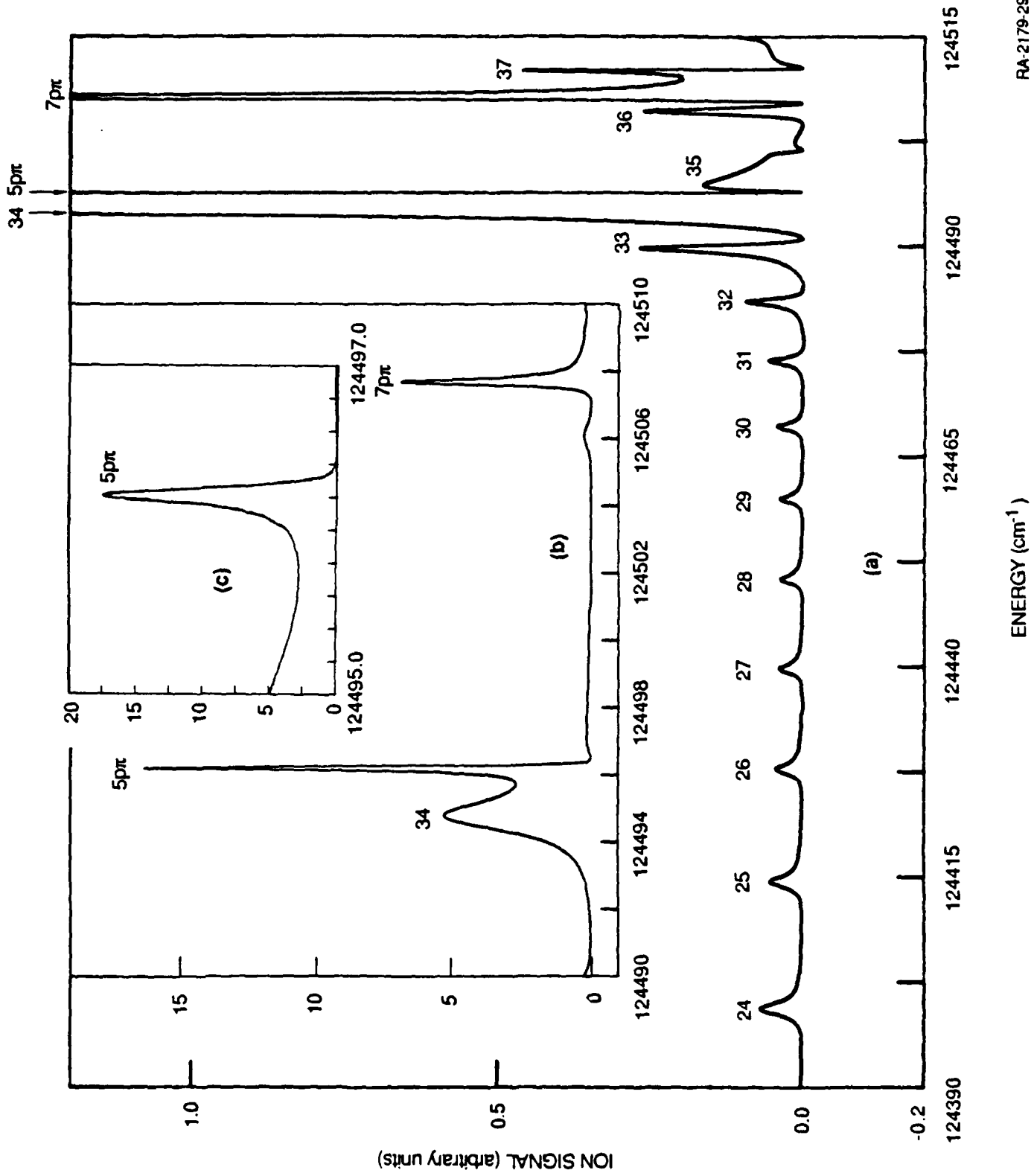


Figure 12

Appendix B

FOUR-PHOTON DISSOCIATION AND IONIZATION OF H₂

Four-photon dissociation and ionization of H₂

E. Y. Xu, T. Tsuboi, R. Kachru, and H. Helm

Molecular Physics Department, SRI International, Menlo Park, California 94025

(Received 20 July 1987)

We report a quantitative investigation of competition between dissociation and ionization in four-photon excited H₂. The C ¹Π_u v=0-4, N=1-3 states are prepared by three-photon excitation from the ground state. Absorption of a fourth photon from the same laser pulse leads either to H₂⁺+e or H+H(n=3,4). This branching is monitored in photoelectron spectra, taken with a novel magnetic bottle electron spectrometer based on a permanent magnet design. The competition between dissociation and ionization shows a pronounced dependence on the symmetry, vibrational, and rotational quantum numbers of the C state. We attempt to explain this dependence in terms of excitation of dissociative H₂ states in the H₂⁺ ionization continuum from which both autoionization and dissociation may occur.

I. INTRODUCTION

The energy region above the lowest ionization limit of a molecule generally also lies above the lowest dissociation threshold. Excitation of the molecule to this energy regime involves configurations for which two dynamic events, dissociation and ionization, compete. This interplay is illustrated by the dissociative recombination process observed for molecular ions. In the hydrogen molecule, dissociative states which extend into the ionization continuum can be considered as "doubly excited" states or as Rydberg states converging to an electronically excited state of H₂⁺. The lowest of these, 1σ_u² ¹Σ_g⁺, profoundly affects the excited ¹Σ_g⁺ states of the neutral molecule and is responsible for the efficient dissociative recombination of the molecular ion.¹

With the advent of multiphoton excitation experiments, spectroscopic access into this symmetry and this energy domain has become possible and we report here an experimental study which probes the interaction between ionization and dissociation channels in the hydrogen molecule.

Dissociative ionization has been observed in several recent studies on multiphoton resonant ionization of H₂. Pratt *et al.*² reported the observation of a small amount of H(n=2) fragments in multiphoton excitation via the B ¹Σ_u⁺ v=7 state. Bonnie *et al.*³ found the dissociative channel to excited atomic hydrogen to become a dominant decay channel following excitation via the vibrational levels v=8-11 of B ¹Σ_u⁺. In these studies H⁺ ions were formed and the resulting electrons detected when the excited hydrogen atom was photoionized by the excitation pulse. A different mechanism for H⁺ formation was invoked by Bjerre *et al.*⁴ who reported observation of H⁺ in (2+1) photon resonant photoionization of H₂ via the E,F ¹Σ_g⁺ (v=2) state. These authors attributed the dissociation channel to the absorption of a fourth photon by H₂⁺ formed in vibrational levels v≥2. This phenomenon was also detected in E,F-state excitation by Bonnie *et al.*⁵

We have recently observed⁶ extensive dissociation in multiphoton excitation via the C state (v=2) by simultaneously recording the appearance of H⁺ and H₂⁺ ions. Most striking was the fact that dissociative ionization occurred preferentially on R and P branches while it was significantly smaller when multiphoton excitation occurred in the Q branches. The three-photon excitation wavelengths to the C(v=2) level lie near 2900 Å. At these wavelengths only vibrational levels v⁺>5 of H₂⁺ are efficiently photodissociated.⁷ Judging from the photoelectron spectra of Pratt *et al.*⁸ it is clear that four-photon ionization via the C state (v=2) does not populate the higher vibrational levels of the ion and hence photodissociation of the parent ion, H₂⁺, could not be the source of the intense photodissociation channel in v=2 excitation. Moreover, the significant difference in the degree of photodissociation associated with populating the C state via the Q or R,P branch could not easily be explained in terms of direct photodissociation of the primary ionization product, H₂⁺.

To assess the nature of the dissociation process we have examined the energy distribution of photoelectrons produced in photoionization of the intermediate C ¹Π_u v=0-4, N=1-3 states and we report these experiments here. The C-state levels are prepared by three-photon single-color resonant excitation in Q and R transitions. Ionization occurs when additional photons are absorbed from the same laser pulse. Our electron spectra show that transitions from the C state can access dissociative electronic states above the ionization threshold from which both dissociation and autoionization may occur. Our findings have triggered a theoretical treatment of this process.⁹

Concurrent with our study a very detailed photoelectron spectroscopy experiment on the rovibrational distribution of the H₂⁺ ions following (3+1) photon ionization of H₂ via the C state was carried out by O'Halloran *et al.*¹⁰ In these studies the strong non-Franck-Condon distribution of rovibrational levels of the H₂⁺ product ions were examined in beautiful detail and attributed to

the presence of a dissociative electronic state as intermediate in the ionization step to H_2^+ . Also in their studies, observations of dissociation channels were discovered for $v=2$ and 3, however, they were not examined in detail.

The role played by dissociative electronic states in the photoionization dynamics of the hydrogen molecule has been discussed very recently by Chupka.¹¹ Chupka concludes that excitation and autoionization of the doubly excited $^1\Pi_g$ ($2p\sigma_u 2p\pi_u$) state is responsible for the anomalous vibrational distributions observed in resonant multiphoton ionization of H_2 via the C state and he predicts formation of excited atomic hydrogen fragments in the very same process. An extension of this picture is used here to discuss the difference in the ionization properties which we observe in Q , and R branch excitation via the C state.

II. EXPERIMENT

The photoionization experiments were performed in a pulsed hydrogen nozzle beam and the photoelectrons were analyzed using a bottle electron spectrometer. A supersonic jet provides a pulse of gas prior to the time of the laser firing, filling the vacuum chamber which is pumped to 1×10^{-6} torr with an average 2×10^{-6} torr of H_2 gas. A Nd:YAG laser (Spectra-physics DCR-2; where YAG denotes yttrium aluminum garnet) pumps a dye laser (QuantaRay PDL), and the output is frequency doubled to 2800–3000 Å to three-photon excite the H_2 $C^1\Pi_u$ ($v=0-4$) states. The fundamental 6000-Å beam is attenuated by a factor of 10^7 with a 2-mm UG-5 filter, leaving the residual visible light at less than $1 \mu J$ per pulse. The typical energy of the 5-ns uv pulse is 4–8 mJ. The laser is focused by a 20-cm focal-length lens. The excitation spectra are assigned on the basis of the single-photon $C \leftarrow X$ and $B \leftarrow X$ transitions reported by Dabrowski and Herzberg.¹²

The gas jet and laser beam intersect in the high-field region of the magnetic bottle electron spectrometer. The magnetic field configuration is that described by Kruit and Reed,¹³ but permanent magnets and specially shaped pole faces are used to create the high-field region. This magnetic spectrometer is a prototype model of a permanent-magnet design developed during the past year in our laboratory by one of the authors (T.T.). A description of this design will appear in a separate paper.¹⁴ The magnetic field at the interaction center is 9000 G and the field drops to 10 G in 30 mm distance on the flight axis of the spectrometer. This sharp gradient¹³ rotates the velocity vectors of photoelectrons with energies up to several eV; the result is that all electrons going into the 4π -sr section after the multiphoton ionization process are parallel along the magnetic symmetry axis and those emitted in the 2π hemisphere on one side of the flight tube move into a time-of-flight drift region towards a multichannel plate detector. A coil around the 50-cm-long drift region maintains a 10 G field so that the electrons continue to drift (with a small component of helical motion) along the axis until they reach the detector. The electron collecting efficiency has

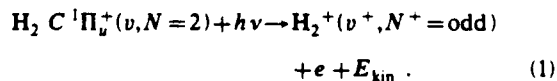
been measured to be near the maximum expected 50%.

Our resolution for recording the time-of-flight (TOF) spectra is ~ 20 ns, to some extent limited by the analog electronics used to record TOF spectra. Electron spectra are averaged on a transient digitizer (Tektronix 7D20) from which the data are transferred to a PDP-11 computer. The time-of-flight spectra are converted into electron energy spectra, taking account of the conversion of electron intensity from unit time interval into unit energy interval. A contact potential effect was observed to retard the electron energy by approximately 250 mV. This is corrected for by calibrating against the known ionization potentials of H_2 (Ref. 15) as well as krypton, which was ionized by (3 + 1)-photon excitation at 2853 Å. No external electric fields were applied. We recognized some wavelength-dependent photoelectron signals due to the photoionization of residual gases in the vacuum system. We took a background measurement following each H_2 measurement and subtracted the background. This subtraction is the origin of the noisy trace in portions of some of the photoelectron spectra. We found no noticeable dependence of the photoelectron distributions on the laser polarization. The polarization was in general kept parallel to the flight-tube axis. We learned, however, as was kindly pointed out to us by Pratt and co-workers, that high laser power and high hydrogen densities which give rise to high photoelectron densities in the excitation volume are primarily responsible for the limited resolution in some of the spectra.

We have also set up a time-of-flight ion spectrometer near the electron chamber. The laser beam is steered into the ion chamber, when needed, to monitor the ionic species produced in the same multiphoton process.

III. RESULTS

Three representative sets of photoelectron spectra resulting from multiphoton excitation of H_2 via the C state are shown in Figs. 1–3. In Fig. 1 the excitation follows a three-photon R 1 transition from the ground vibrational state of H_2 to the $N=2$ rotational levels of the C state ($v=0$ to 3). Owing to selection rules, photoionization to H_2^+ from these C -state levels populates only the orthohydrogen levels of H_2^+ :



The tick marks above the low-energy electron peaks in Fig. 1 indicate the distribution of possible final states from process (1). Figure 1 shows that with increasing vibrational excitation of the C state a contribution of other electron groups appears in the spectra. Their energies correspond to the excess energy imparted in electrons in the photoionization of excited atomic hydrogen,



The energy predicted for process (2) at the respective photon wavelengths is marked below the experimental traces. Since we find the appearance of the atomic ion channel in both the photoelectron and photoion spec-

trum to be resonant with the $C \leftarrow X$ three-photon transition we conclude that the origin for the excited hydrogen fragments is a photodissociation process



which competes with the molecular ionization channel (1). The energy markers for process (2) are shown in Fig. 1 for those excited atomic states which are energetically accessible in a vertical four-photon transition from the ground state. As higher vibrational levels in the C state are accessed, channels with increasingly higher n values open for the fourth photon in reaction (3), and they are indeed populated. There is, however, no clear indication in these spectra that $\text{H}(n=2)$ is formed in significant quantity.

The width of the electron energy peaks in Fig. 1 for the atomic photoionization process are wider than those arising from the molecular ion channel. This is due to

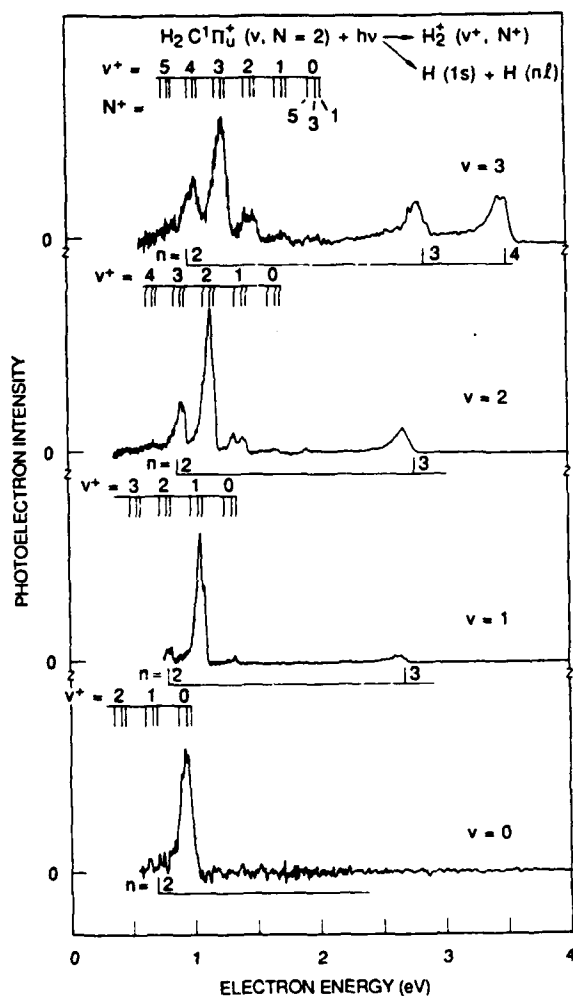


FIG. 1. Photoelectron energy spectra recorded at the wavelengths for three-photon resonant $\text{C}^1\Pi_u(v=0-3) \leftarrow \text{X}^1\Sigma_g^+(v=0)$ excitation via the R1 transition. Photoelectron intensity is in arbitrary units.

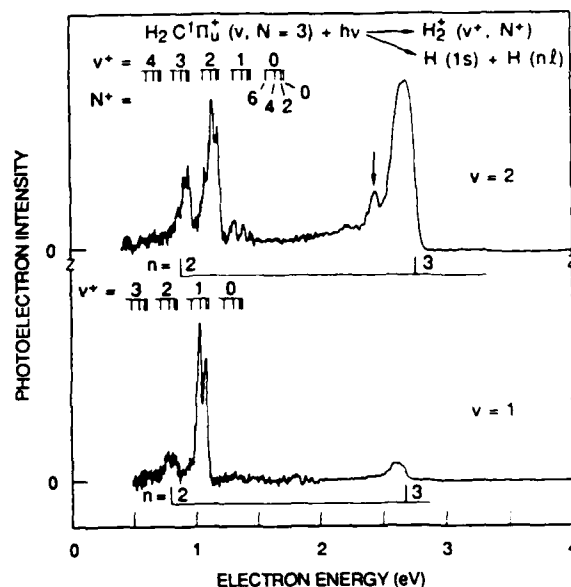


FIG. 2. Photoelectron energy spectra recorded at the wavelengths for three-photon resonant $\text{C}^1\Pi_u(v=1,2) \leftarrow \text{X}^1\Sigma_g^+(v=0)$ excitation via the R2 transition. Photoelectron intensity is in arbitrary units.

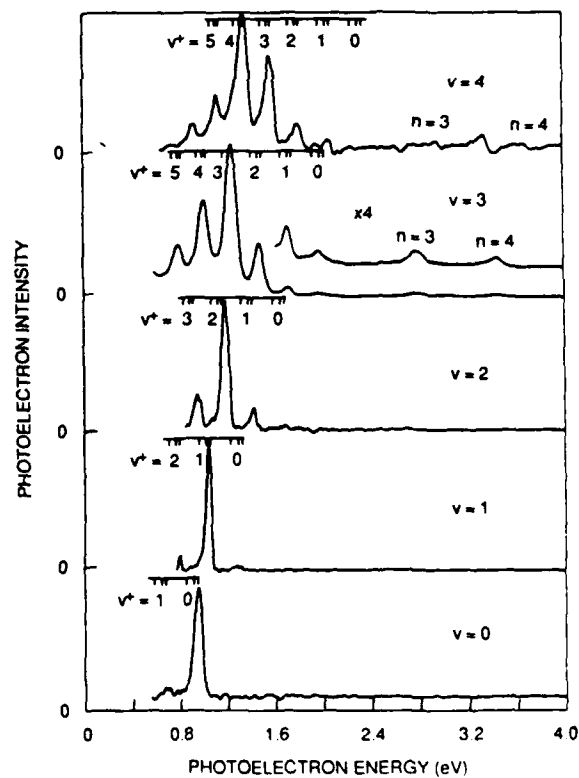


FIG. 3. Photoelectron energy spectra recorded at the wavelengths for three-photon resonant $\text{C}^1\Pi_u(v=0-4) \leftarrow \text{X}^1\Sigma_g^+(v=0)$ excitation via the Q1 transition. Photoelectron intensity is in arbitrary units.

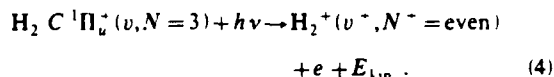
the time-of-flight method used here which has nearly constant time resolution at all electron energies. Hence, at higher electron energies this finite time resolution translates into a correspondingly larger energy breadth. The asymmetry in the time-of-arrival peaks (which is reflected by the asymmetry of the peaks in the energy spectra) is an inherent feature of the magnetic bottle spectrometer,¹³ its origin lies with the angular distribution of photoelectrons, and the finite time it takes to bend electron trajectories in the high-field region.

To assess the relative importance of dissociation over formation of H_2^+ we have integrated over the respective parts of the photoelectron spectra. The results are given in Table I. We observed that the relative signal of electrons from process (2) increased slightly (less than linear) when we increased the laser intensity within our experimental availability. Since our nominal photon flux in the ionization volume is sufficient to saturate the atomic ionization channel we conclude that the small increase is due to boundary effects in the ionization volume. As a result the branching ratios given in Table I strictly represent only lower limits for the degree of dissociation of four-photon excited H_2 .

In Fig. 2 we show electron energy spectra which appear in the multiphoton excitation of the C state via the $R2$ transitions to the vibrational levels $v=1$ and 2. In this process only even rotational levels of H_2^+ (parahydrogen) can be populated

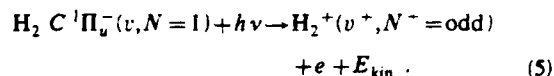
TABLE I. Ratio of dissociation into $H(n=3)+H(n=4)$ to formation of H_2^+ in $(3+1)$ -photon resonant excitation of H_2 via the $C^1\Pi_u^+$ state. Values are given for the percentage B -state character acquired in mixing of the Π^+ levels with the nearest-neighbor B -state level. Excitation wavelengths (λ_{vac} , Å) are obtained from the tabulation of Dabrowski and Herzberg (Ref. 12). The ratios represent lower limits for the degree of dissociation (see text for details).

Transition level	Dissociation-ionization	B -state character	Excitation wavelength
$Q1 v=0$	~0	0	3029.31
$Q1 v=1$	<0.02	0	2960.39
$Q1 v=2$	<0.02	0	2898.29
$Q1 v=3$	0.03	0	2842.39
$Q2 v=3$	0.07	0	2845.85
$Q1 v=4$	~0.10	0	2791.72
$R1 v=0$	~0	0.08	3025.50
$R2 v=0$	~0	0.17	3027.09
$R1 v=1$	0.12	0.20	2956.95
$R2 v=1$	0.20	0.60	2959.74
$R1 v=2$	0.16	1.6	2895.20
$R2 v=2$	~0.95	12.0	2897.38
$R1 v=3$	0.55	13.0	2839.16
$R1 v=4$	0.04	1.1	2789.06



Rotational resolution is achieved for the final H_2^+ states in Fig. 2. In addition to photoelectrons from process (4) an important contribution of electrons from photoionizing $H(n=3)$ appears in these spectra. Comparing Figs. 1 and 2 we see that the degree of dissociation is higher on the $R2$ transitions.

The pronounced branching between the formation of H_2^+ and $H(nl)$ in $R1$ and $R2$ transitions is in strong contrast to the properties of $Q1$ line excitation via the C state. In Fig. 3 we show photoelectron spectra obtained on the $Q1$ transitions to $v=0$ to 4 of the C -state. In the Q branch the Π^- component of the C state is accessed and its photoionization follows almost exclusively via the process



A minor dissociation channel is observed for the transition via $v=3$ of the C state, the magnitude of dissociation being similar to that found in Fig. 3 of Ref. 8. Some dissociation appears to be present in the $v=4$ spectrum as well. The noisy trace in this spectrum is due to a resonant background gas ionization channel at this wavelength. While this prevents us from determining a precise value for the dissociated fraction it is evident that dissociation in $v=4$ is not substantially higher than in $v=3$.

The marked difference in the photoionization paths for Q - and R -branch excitation via the C state as evident from Figs. 1-3 suggests that the difference arises from selection rules that govern the absorption of the fourth photon. The symmetry properties of the C state when populated via the Q branch are Π^- , with the dominant orbital configuration being $1s\sigma_g 2p\pi_u$. On the other hand, R -branch excitation prepares the $C^1\Pi_u^+$ state. Its configuration is also $1s\sigma_g 2p\pi_u$, but the Π^+ species is rotationally coupled with $1s\sigma_g 2p\sigma_u$, the configuration of the $B^1\Sigma_u^+$ state. The $B^1\Sigma_u^+$ $v=8$ to 16 states lie in the vicinity of the $v=0$ to 4 levels of C state, and perturbations between the Π^+ and B -state levels have been well documented.¹²

Previous experiments conducted by Bonnie and co-workers³ have shown that dissociation is a dominant process following four-photon excitation of H_2 , when vibrational levels $v=8$ to 11 are pumped in the B state. The similarity in the dissociation behavior of four-photon excited H_2 via the R branches of the C state and via the B state suggests that the dissociation mechanisms in the two cases may be related and fundamentally different from the very much weaker dissociation path observed for the higher vibrational levels of the C state when excited in a Q branch. To exemplify the dominance of dissociation in excitation via the B state we show in Fig. 4 a photoelectron spectrum obtained via the $B^1\Sigma_u v=14 R1$ transition. The two main peaks here arise from photoionization of $H(n=3,4)$ formed by photodissociation of $H_2 B(v=14, N=2)$. A smaller number

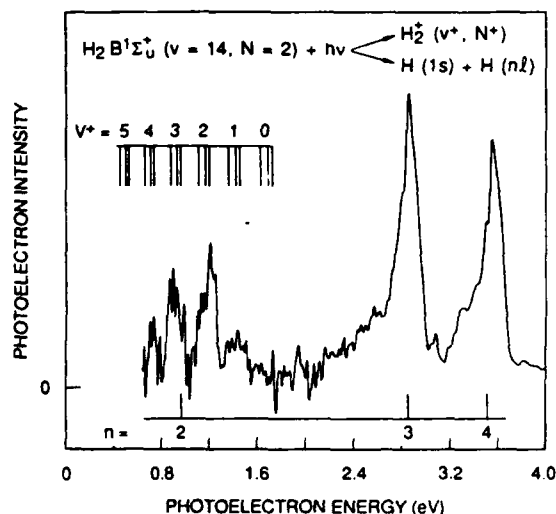


FIG. 4. Photoelectron energy spectrum resulting from three-photon resonant excitation of the $B^1\Sigma_u^+(v=14)$ via the R1 transition ($\lambda_{vac}=2840.96$ Å). Photoelectron intensity is in arbitrary units.

of electrons results from formation of H_2^+ in the vibrational levels $v=2$ and 3 , as indicated by the markers above the trace.

Two additional features in the spectra deserve comment. For one, it appears that the dissociative channel into $H(n=2)$, if present at all, is weaker than observed for $H(n=3)$ and $H(n=4)$. In nearly all cases the $n=2$ electron energy from process (2) overlaps with electrons expected from ionization into H_2^+ and we are unable to assess its absolute contribution. The branching ratios in Table I do not include the $n=2$ energy region as part of the dissociative fraction. It must be noted also that the detection efficiency for $H(n=2)$ is expected to be smaller than that for the higher limits since the faster $n=2$ fragments are more likely to escape from the ionization volume during the duration of the laser pulse.

A second point is the additional peak at ~ 2.5 eV in the $v=2$ spectrum of Fig. 2. The peak is marked by an arrow and it lies ~ 270 meV lower in energy than the large $n=3$ dissociation peak. The peak position does not fit into a feasible mechanism that we could think of in H_2 . We investigated several experimental conditions such as H_2 sample purity, the laser polarization, laser power, and H_2 gas pressure. The intensity of this 2.5-eV peak relative to the $n=3$ signal appeared independent of these experimental conditions and the peak appeared in wavelength concurrent with the $n=3$ peak. The peak is not part of the background spectrum which is taken with laser on but without operating the H_2 gas valve. Since we also found it impossible to attribute the peak to the natural deuterium content of hydrogen or collisions with ground-state H_2 gas, we conclude that it is either due to an impurity introduced via the pulsed valve or a consequence of an inelastic (vibrational) energy loss in collisions of $n=3$ electrons with impure background gas in the high magnetic field region.

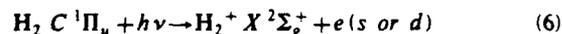
IV. DISCUSSION

To facilitate discussion of the observed effects we show in Fig. 5 potential energy curves relevant for the excitation scheme via the $C^1\Pi_u$ state. The equilibrium separation of $H_2 X^1\Sigma_g^+ v''=0$ lies at shorter R than that of the $C^1\Pi_u$ state. As a result good Franck-Condon factors exist for transitions from the ground state to various vibrational levels of the C state. The $C^1\Pi_u$ state molecular potential, however, almost overlaps in shape with the ground state of H_2^+ , $X^2\Sigma_g^+$. Therefore the Franck-Condon overlap between the two states will strongly favor transitions with $v-v^+=0$. As has been discussed in detail previously,^{8,10,11,16} direct ionization of a pure C state into H_2^+ , in the absence of autoionizing states, should closely follow the Franck-Condon selection rules. This is in contrast to what was observed experimentally.^{8,10} Our results shown in Fig. 3 reiterate these previous observations. All photoelectron spectra in Q1 excitation (where a "pure" C state is populated) show substantial contributions from electrons emitted at energies corresponding to $v-v^+\neq 0$. For example, in $v=4$ excitation the $v^+=3$ peak amounts to 75% of the $v^+=4$ peak, and the $v^+=5$ peak is 35% of the $v^+=4$ peak, compared with Franck-Condon factors⁸ of 5% for both $v^+=3$ and $v^+=5$ formation.

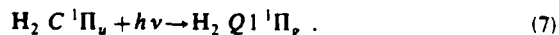
An explanation for this behavior has been advanced by Chupka¹¹ and formulated theoretically by Hickman.⁹ Both authors recognize the importance of doubly excited states¹⁶ of H_2 in the ionization process. The non-Franck-Condon distribution appears intimately connected with the appearance of dissociation in four-photon excited H_2 . We discuss in the following the likely origins of photodissociation.

A. The doubly excited $^1\Pi_g$ state

Photoexcitation of a pure C state occurs either in a direct process, whereby the $2p\pi_u$ orbital is excited into the continuum



or in a "core-type" excitation $1s\sigma_g \rightarrow 2p\sigma_u$:



In the latter case the excitation is similar to the bound-free photodissociation process observed for H_2^+ . The doubly excited $Q1^1\Pi_g$ state (configuration $2p\sigma_u 2p\pi_u$) has been calculated by Guberman¹⁷ and his result is included in Fig. 5. This state may be viewed as a Rydberg state converging to the repulsive $A^2\Sigma_u^-$ state of H_2^+ . When excited in a vertical transition from the C state the $Q1^1\Pi_g$ lies in the ionization continuum of ground-state H_2^+ . Hence, during dissociation, this configuration may autoionize. Even after passing the critical distance for this process, which is the intersection of the $H_2^+ X^2\Sigma_g^+$ and $Q1^1\Pi_g$ potential energy curves, the molecule is not free to merely dissociate. The reason is (see Fig. 1 of Chupka¹¹) that the outgoing $Q1$ state intersects a multitude of avoided crossings with the bound gerade Rydberg states from which autoioniza-

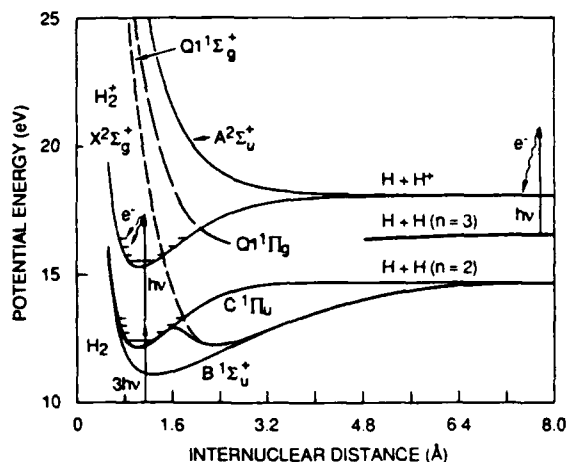


FIG. 5. Potential energy curves of H_2 relevant to our resonant multiphoton excitation scheme. The straight arrows represent the final photons absorbed. The wiggly arrows symbolize the emitted electrons and their corresponding kinetic energies.

tion may occur.

The competition between dissociation and ionization into H_2^+ in the multiphoton excitation process is governed by the excitation probability for accessing the $Q1$ state versus process (6) and the probability that the doubly excited state survives autoionization. Chupka¹¹ has compared the calculated¹⁸ ionization cross section for process (6) with the cross section for photodissociation of ground-state H_2^+ . The latter process involves similar transition moment and potential energy curves as the excitation process (7). We have calculated¹⁹ the cross section for process (7) using the potential energy curve of the $Q1^1\Pi_g$ state given by Guberman¹⁷ and that of the C state given by Wolniewicz,²⁰ taking the transition moment as $R/2$, as appropriate for the $1s\sigma_g \rightarrow 2p\sigma_u$ excitation.⁷ The result is indeed similar to the photodissociation cross section of H_2^+ and it is shown in Fig. 6 for the lowest five vibrational levels of the C state. The calculations were carried out for different rotational quantum numbers. The results for $N=1$ and $N=3$ are given in our figure. In the wavelength region of interest here the cross sections increase by less than a factor of 2 when going from $N=1$ to 3, the rotational dependence being much smaller than the vibrational variation.

Comparing these cross sections with that for direct photoionization¹⁸ (indicated by the dashed line in Fig. 6), we see that for low vibrational levels (in the wavelength range predetermined by the resonant excitation to the C state) the indirect path via the doubly excited state is of low probability, but should become significant for the vibrational levels $v=3$ and 4. Care has to be taken in using the absolute values of the excitation cross sections. They are sensitive to the absolute energy of the $^1\Pi_g$ potential energy curve (an energy shift of the curve translates in the first order into a corresponding shift on the wavelength scale) and to the autoionization width of the $^1\Pi_g$ state. This width has been predicted by Bottch-

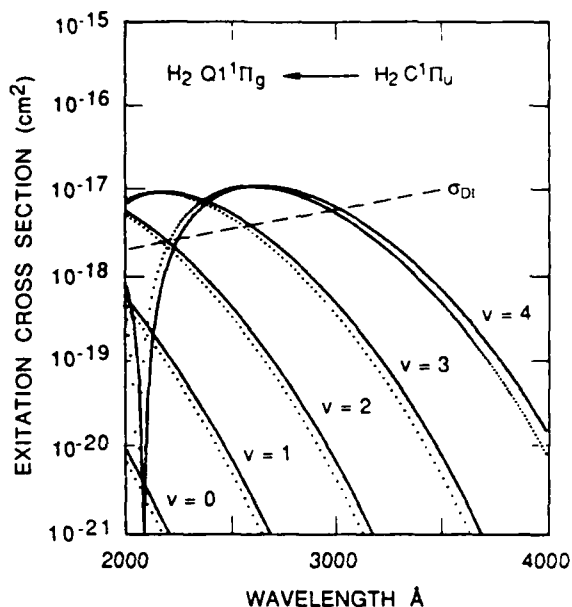


FIG. 6. Calculated cross section for photoexcitation of the $Q1^1\Pi_g$ state from the vibrational levels $v=0$ to 4 of $C^1\Pi_u$. The dotted line gives the result for the rotational quantum number $N=1$ of the C state, the solid curve gives the cross section for $N=3$. The dashed line is the direct photoionization cross section given in Ref. 18.

er²¹ to be 0.2 eV. Introduction of this width into the cross section would lead to a small decrease in the cross section maxima and a slight smoothing of the oscillatory features.

Taking the cross sections in Fig. 6 at face value we predict that for $v=3$ the ratio of excitation of the $^1\Pi_g$ state to direct ionization is 0.17, while it is 1.4 for $v=4$. These values may be compared with our observation of a ratio of dissociation to ionization of about 0.03 in the $Q1$ transition via $v=3$, and roughly 0.10 via $v=4$. The difference between the two sets of numbers obviously reflects the fact that autoionization of the $^1\Pi_g$ state is significant. Hickman⁹ who takes explicit account of the survival probability of the $^1\Pi_g$ state against autoionization predicts a ratio of 0.016 for $v=3$ and 0.056 for $v=4$.

A second comparison that can be made involves the rotational dependence of the dissociated fraction. For $v=3$ we have measured this fraction for both $Q1$ and $Q2$ line excitation (see Table I). The magnitude of this increase is not reflected by the rotational dependence of the excitation cross section of the $Q1^1\Pi_g$ state (Fig. 6). Our calculations predict the photoexcitation probability for process (7) to increase by only $\sim 10\%$ at the respective wavelengths for $v=3$ excitation when the rotational quantum number of the C state increases from $N=1$ to $N=2$. Thus we are led to conclude that the autoionization probability of the doubly excited state may depend on rotation.

Nevertheless, it appears that within experimental and

theoretical uncertainties the degree of dissociation that is observed in (3 + 1) photon resonant ionization via the Π^- levels can reasonably be accounted for by invoking excitation of the C state to the $Q1^1\Pi_g$ state.

This is not the case for excitation via the Π^+ levels where dissociation is significant already for $v=1$, and comparable to ionization for the higher vibrational levels. We explore in the following two possible origins for the increased degree of dissociation observed for H₂ that is four-photon excited via the Π^+ levels.

B. Photodissociation of Π^+ levels of the C state

Just as the Π^- levels do, the Π^+ levels connect in an allowed transition with the doubly excited $^1\Pi_g$ state. The strongest transitions from the C-state to the doubly-excited state occur in P- and R-type branches, both of which populate Π_g^+ from Π_u^+ and Π_g^- from Π_u^- . Judging from the location of the doubly excited $^1\Sigma_g^+$ states among Guberman's curves,¹⁷ the Λ -type splitting between Π_g^+ and Π_g^- can hardly exceed the wavenumber domain. As a result we may assume the probability of excitation to the doubly excited $^1\Pi_g$ state to be equal for both C-state components. As is evident from Fig. 6 any substantial degree of dissociation in $v=1$ (as seen near 2960 Å in Figs. 1 and 2) would require a significant increase in this cross section. The sheer magnitude of dissociation seen for the Π^+ component at low vibrational levels is inconsistent with the excitation cross section in Fig. 6, even if the survival rate against autoionization is taken as 100%.

Raising the excitation cross section in Fig. 6 to a level required to explain the observed photodissociation of the Π_u^+ components could indeed be accomplished by lowering Guberman's $Q1^1\Pi_g$ curve by ≥ 0.5 eV. This lowering would bring about a concurrent increase in the rate of dissociation of the Π^- levels. To achieve qualitative agreement with the experimental observations, the difference in dissociation for the two C-state components would have to be blamed on a difference in the autoionization rates of the doubly excited Π_g^+ and Π_g^- components. The autoionization process of $Q1^1\Pi_g$ is a consequence of the two-electron process



It can only be expected to be different for Π_g^+ and Π_g^- in the event of severe Λ -doubling distortion of the configuration on the left hand side of (8).

A second and more attractive path appears to rest with the B-state admixture of the $C^1\Pi_u^+$ components. The percentage B-state character of individual $C^1\Pi_u^+$ levels can be estimated to first order by using two-state perturbation theory between the C-state levels and their nearest neighbors in the B state. Using the level positions and rotational coupling matrix elements given by Dabrowski and Herzberg¹² we found the values included in Table I. It can be seen that for each given v the fraction of photodissociation does indeed follow the admixed B-state character. For a quantitative comparison of the mixing factor with the measured dissociation rates of the

Π^+ levels, the photoionization-photodissociation properties of the nearest B-state neighbor have to be known. We have obtained experimental data for one such case: The $v=3, N=2$ level in the C state has a predicted B-state admixture of 13%. This high degree of mixing arises from the proximity (67 cm^{-1}) of the B-state level $v=14, N=2$. The ratio measured for the two paths, dissociation-ionization amounts to 0.55 for this C-state level (see Fig. 1, top trace). By comparison, the close-lying B-state neighbor perturbing this level, $v=14, N=2$, is photoexcited at very nearly the same wavelength. Its photoelectron spectrum is shown in Fig. 4. For this (87% "pure") B state the ratio of dissociation over ionization amounts to 3.8, a factor of ~ 7 higher than that seen for the neighboring (13% "mixed") C state. We conclude from this comparison that mixing with the B state will indeed play a major role in the photoionization dynamics of the $C^1\Pi_u^+$ states. It remains to explain the origin for the dominant dissociation path observed for the higher vibrational levels of the B state.

C. Photodissociation of $B^1\Sigma_u^+$

A prime candidate upper state for B-state photodissociation appears to be the lowest doubly excited state, $Q1^1\Sigma_g^+$, configuration $(2p\sigma_u)^2$. This state, as calculated by Guberman,¹⁷ is shown in Fig. 5. Outside the H₂⁺ continuum his potential energy curve smoothly joins the outer well of the $E,F^1\Sigma_g^+$ state which we also included in Fig. 5. Outside the ionization continuum this doubly excited state finds continuation also in the undulations of the $GK, H\bar{H}$ states²² and corresponding $^1\Sigma_g^+$ potentials arising from the $n=3$ and 4 dissociation limits. Using Guberman's diabatic $^1\Sigma_g^+$ state without accounting for its large autoionization width (1.2 eV, Ref. 1) we have calculated the bound-free absorption cross section for the B state ($v=8$ to 14) to be $\sim 1 \times 10^{-18} \text{ cm}^2$ in the wavelength region between 2000 and 3000 Å. This small cross section together with the relatively minor B-state admixture acquired by the $C^1\Pi_u^+$ levels considered in Table I, seem to exclude the possibility that the perturbed C-state levels dissociate to a significant degree via the doubly excited $^1\Sigma_g^+$ state.

A second path for photodissociation of the B state is via the continuum of the $^1\Sigma_g^+$ double-well states. Using the transition moments and potential energy curves for the $EF, GK,$ and $H\bar{H}$ states given by Wolniewicz and Dressler²² we have calculated these cross sections. In the wavelength region of interest here none of them exceeds $5 \times 10^{-19} \text{ cm}^2$. Therefore we also exclude these states as being the sole source of photodissociation of the perturbed C components. No experimental information appears available on the higher lying $^1\Sigma_g^+$ states arising from the $n=3$ and 4 limits which are accessible in photoabsorption from the B state. It is conceivable that these higher-lying states will show an enhanced absorption cross section due to the better bound-free overlap at our photon energies.

However, the B state may also access the doubly excited $Q1^1\Pi_g$ state in an allowed transition. We have calculated the corresponding excitation cross section using as

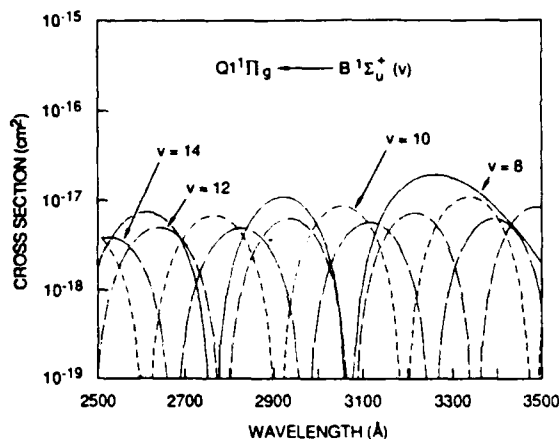


FIG. 7. Calculated cross section for excitation of $Q1^1\Pi_g$ from the vibrational levels $v=8, 10, 12,$ and 14 of $B^1\Sigma_u^+$. The rotational quantum number of the B state is $N=2$.

transition moment the atomic ($2p \leftarrow 1s$) value of 1.66.²³ The results are given in Fig. 7 for the vibrational levels $v=8, 10, 12,$ and 14 . These vibrational levels lie close in energy to the $v=0$ to 4 levels of the C state. The B -state cross section is on the average higher than that for the C state (Fig. 6) but oscillates rapidly with wavelength as a result of the high vibrational levels considered. These rapid oscillations make the absolute value of the cross section extremely sensitive to the exact location of the $Q1^1\Pi_g$ potential energy curve. The magnitude of this cross section has to be compared with the fact that direct ionization of the higher B -state levels into H_2^+ is attenuated due to poor Franck-Condon overlap. This suggests that bound-free photodissociation via the doubly excited $^1\Pi_g$ state will significantly influence the photoabsorption of the B state.

The fragmentary knowledge about the various excitation channels of the B state does not warrant at this time estimating its quantitative contribution to photodissociation of the perturbed Π^+ components. However, we feel that the accumulated evidence proves in sufficient detail that the difference observed in Q - and R -branch excitation of H_2 via the C state originates from the mixing of the Π_u^+ components with the $B^1\Sigma_u^+$ state. A precise quantitative calculation will have to entail a proper account of the coherent excitation of the adiabatic $^1\Sigma_g^+$

and $^1\Pi_g$ states and the competition of dissociation with direct ionization and autoionization channels.

V. CONCLUSIONS

We have presented experimental photoelectron spectra on the $(3+1)$ -photon ionization and dissociation of H_2 via the $C^1\Pi_u$ $v=0-4, N=1-3$ excited states. We observe a significant dependence of the competition between ionization and dissociation of four-photon excited H_2 on the quantum numbers of the resonant intermediate C states.

We interpret our findings in terms of excitation of doubly excited states in the ionization continuum of H_2^+ , from which both autoionization and dissociation can occur. Our observations can qualitatively be accounted for in the case of resonant excitation via the Π^- levels, the "pure" C state, in which case the fourth photon accesses the $Q1^1\Pi_g$ state.

The situation is more complex for the "mixed" Π^- levels. Rotational mixing opens additional dissociative decay channels which are closed to the Π^- component, but which govern the excitation dynamics of the $B^1\Sigma_u^+$ state. Our model calculations predict that among the open channels the $Q1^1\Pi_g$ state plays a major role. At the wavelengths involved here excitation of this state from $B^1\Sigma_u^+$ has a larger cross section than from $C^1\Pi_u$, primarily a result of the larger internuclear distances involved for the B state. This fact may also suppress autoionization of the $Q1^1\Pi_g$.

Our experiments demonstrate that dissociative electronic states in the ionization continuum, which play an important role in dissociative recombination, are spectroscopically accessible in multiphoton excitation. Most powerful would be an experiment in which a laser is scanned through the dissociation region, following excitation of a single discrete H_2 level. The authors are preparing such an experiment.

ACKNOWLEDGMENTS

We gratefully acknowledge stimulating advice from Dr. D. L. Huestis and Dr. R. P. Saxon. We wish to thank Dr. Chupka and Dr. O'Halloran for supplying copies of their work prior to publication. The research was supported by the U.S. Air Force Office of Scientific Research (AFOSR) under Contract No. F49620-86-K-0017.

¹A. U. Hazi, C. Derkits, and J. N. Bardsley, *Phys. Rev. A* **27**, 1751 (1983).

²S. T. Pratt, P. M. Dehmer, and J. L. Dehmer, *J. Chem. Phys.* **78**, 4315 (1983).

³J. H. M. Bonnie, J. W. J. Verschuur, H. J. Hopman, and H. B. Van Linden Van der Heuvell, *Chem. Phys. Lett.* **130**, 43 (1986).

⁴N. Bjerre, R. Kachru, and H. Helm, *Phys. Rev. A* **31**, 1206 (1985).

⁵J. H. M. Bonnie, P. J. Eenshuistra, J. Los, and H. J. Hopman,

Chem. Phys. Lett. **125**, 27 (1986).

⁶E. Y. Xu, T. Tsuboi, R. Kachru, and H. Helm, in *Proceedings of the 1987 Western Spectroscopy Conference at Asilomar, CA*, and in *Proceedings of the Division of Atomic, Molecular, and Optical Physics 1987 Conference, Cambridge, MA* (unpublished).

⁷G. H. Dunn, *Phys. Rev.* **172**, 1 (1968).

⁸S. T. Pratt, P. M. Dehmer and J. L. Dehmer, *Chem. Phys. Lett.* **105**, 28 (1984).

⁹A. P. Hickman, *Phys. Rev. Lett.* **59**, 1553 (1987).

- ¹⁰M. A. O'Halloran, S. T. Pratt, P. M. Dehmer, and J. L. Dehmer, *J. Chem. Phys.* **87**, 3288 (1987).
- ¹¹W. A. Chupka, *J. Chem. Phys.* **87**, 1488 (1987).
- ¹²I. Dabrowski and G. Herzberg, *Can. J. Phys.* **52**, 110 (1974).
- ¹³P. Kruit and F. H. Read, *J. Phys. E* **16**, 313 (1983).
- ¹⁴T. Tsuboi, Y. K. Bae, and K. T. Gillen (unpublished).
- ¹⁵G. Herzberg, and C. Jungen, *J. Mol. Spec.* **41**, 425 (1972).
- ¹⁶S. N. Dixit, D. L. Lynch, and V. McKoy, *Phys. Rev. A* **30**, 3332 (1984).
- ¹⁷S. L. Guberman, *J. Chem. Phys.* **78**, 1404 (1983).
- ¹⁸A. Cohn, *J. Chem. Phys.* **57**, 2456 (1972).
- ¹⁹Calculations are based on a bound-free program by P. S. Herman and K. M. Sando, *J. Chem. Phys.* **68**, 1153 (1978).
- ²⁰L. Wolniewicz, *J. Chem. Phys.* **51**, 5002 (1969).
- ²¹C. Bottcher, *J. Phys. B* **9**, 2899 (1976).
- ²²L. Wolniewicz and K. Dressler, *J. Mol. Spectrosc.* **67**, 416 (1977); **77**, 286 (1979).
- ²³H. A. Bethe and E. E. Salpeter, *Quantum Mechanics of One- and Two-Electron Atoms* (Springer-Verlag, Berlin, 1959), p. 264.

Appendix C

FORCED ROTATIONAL AUTOIONIZATION OF
HIGH-LYING STATES OF H₂

Forced rotational autoionization of high-lying states of H_2

Emily Y. Xu, Hanspeter Helm, and Ravinder Kachru

Chemical Physics Laboratory, SRI International, Menlo Park, California 94025

(Received 4 December 1987)

We report the observation of forced rotational autoionization of Rydberg states lying below the lowest ionization threshold of H_2^+ , when a small external electric field is applied. Our observations are accounted for by an intuitive classical ionization model which relates the autoionization process to the lowering of the ionization threshold with the applied field.

Autoionization¹⁻⁷ involves the exchange of energy between a bound excited electron and the core to which the electron is attached. The study of autoionizing states elucidates the anisotropic interactions between the electron and the core at short distances.⁶ In the absence of an external field, autoionization does not occur for states that lie below the lowest ionization threshold of the atom or the molecule. However, these states can be made to ionize in an external electric field. The application of the external electric field depresses the ionization threshold by producing a Stark continuum into which autoionization may occur, in the same manner as above threshold. This phenomenon, which was first discovered by Garton, Parkinson, and Reeves⁸ in Ba, has been termed forced autoionization. In a molecule, the motion of the electron is coupled to electronic, vibrational, and rotational degrees of freedom of the ion core and it should, therefore, be possible to "force" the rotational and vibrational autoionization of the bound Rydberg electrons on excited core states. Such processes were first observed by Dehmer and Chupka⁹ in H_2 and later by Janek, Mullins, Mahon, and Gallagher¹⁰ and Knight, Sohl, Zhu, and Wang¹¹ in Li_2 and H_2 , respectively.

In this Rapid Communication, we report a first systematic study of rotational autoionization of rotationally excited Rydberg states of H_2 , lying below the lowest ionization threshold of H_2^+ , when a small external electric field (~ 15 V/cm) is applied. Specifically, we have observed rotational autoionization of $n=22, 23, 24,$ and 25 states of the para- H_2 series converging to the limit H_2^+ ($N=2$), called the npz series, shown in Fig. 1, and of the $19p$ ortho- H_2 state. These states lie below the lowest rotational state $N=0$ ($N=1$) of H_2^+ and converge to the first excited rotational state, $N=2$ ($N=3$) of the H_2^+ ion core. In order to elucidate a simple intuitive model for the process of forced rotational autoionization, we have determined the dependence of the rotational autoionization signal for the $23p2$ and $22p2$ states on the external electric field. We have also observed rotational autoionization of the members of the np Rydberg series converging to the $N=2$ rotational limit of H_2^+ , which lie above the $N=0$ threshold when these states are excited from the $v'=0, J'=2$ level of the $E, F^1\Sigma_g^+$ state. In this case, the bound channel is primarily excited, and the rotationally autoionizing series appears in the form of bound resonances. In contrast, when the same np states are excited from the $J'=0$ level of the E, F state, the continuum character of the wave function is primarily excited and the

series appears as window resonances or Beutler-Fano profiles⁷ with the Fano q parameter of 0. This is the first time the same state has been observed both as window resonance and as a regular resonance, in a molecule.

The experimental arrangement consists of a pulsed supersonic H_2 beam, which is turned on for ~ 100 μ s. The pulsed H_2 beam passes between two field plates, spaced 0.5 cm apart. The H_2 beam is intersected near the center of the plates by two counterpropagating tunable dye laser beams which are focused by lenses of 15-cm focal length. The first dye laser beam, with $\lambda_1=200-201$ nm is produced by frequency-doubling the output of a tunable dye laser, and then Raman shifting to the fourth anti-Stokes order in a high-pressure H_2 cell. The second dye laser is pumped by an independent Nd-doped yttrium aluminum garnet laser so that the second dye laser can be delayed in time with respect to the first one. The first dye laser with

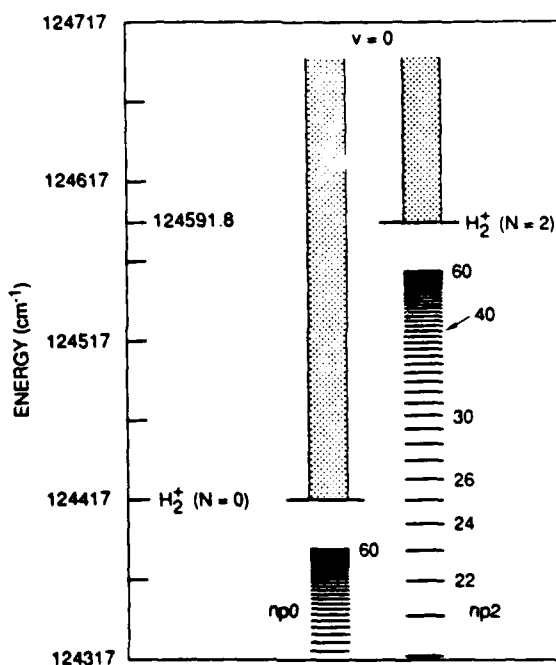


FIG. 1. Energy-level diagram of the H_2 $J=1$ $np0$ Rydberg states converging to the H_2^+ ($N=0$) ionization limit and the $np2$ states converging to the H_2^+ ($N=2$) limit. In this figure, the nearly degenerate $J=1, 2,$ and 3 $np2$ states are shown degenerate.

a typical energy of $100 \mu\text{J/pulse}$ and a spectral width of 1 cm^{-1} , excites the H_2 molecules in a two-photon process from the initial $v''=0, J''=0(2) X^1\Sigma_g^+$ ground state to the $v'=0, J'=0(2) ^1\Sigma_g^+ E, F$ excited state.¹² The second dye laser, with $\lambda=398\text{--}403 \text{ nm}$, spectral linewidth of 0.5 cm^{-1} , and energy of $500 \mu\text{J/pulse}$, subsequently excites the molecule from the selected E, F state in the region around the lowest ionization threshold (see Fig. 1).

In the interaction region, a minimum dc electric field of 15 V/cm is always applied to remove the group of ions formed as a result of photoionization from the first laser and to separate them in time from the group of ions produced by the absorption of the second laser pulse. Figure 2 shows the excitation ion spectrum obtained when the second dye laser is scanned from $398\text{--}401 \text{ nm}$ to excite from $J'=2$ levels of the $v'=0 E, F$ state to the Rydberg states in the region around the ionization threshold. The progressively decreasing spacing between the resonances in the ion spectra in Fig. 2 shows the $np2$ Rydberg states converging to the $\text{H}_2^+(N=2)$ limit. The position of the resonances and their quantum defects relative to the $N=2$ limit⁷ show that the ion resonances in Fig. 2 are the np Rydberg states converging to the $\text{H}_2^+(N=2)$ limit excited in the presence of a small (15 V/cm) electric field. The most striking observation in Fig. 2 is the appearance of the $n=24$ and 25 members of the np series even though they lie 2.2 and 16.3 cm^{-1} below the lowest $\text{H}_2^+(N=0)$ ionization limit. Furthermore, we have observed the onset of forced rotational autoionization of the $23p$ or $22p$ state as the electric field is increased.

At sufficiently high n , the electron-core rotational interaction becomes negligible and states of different J with

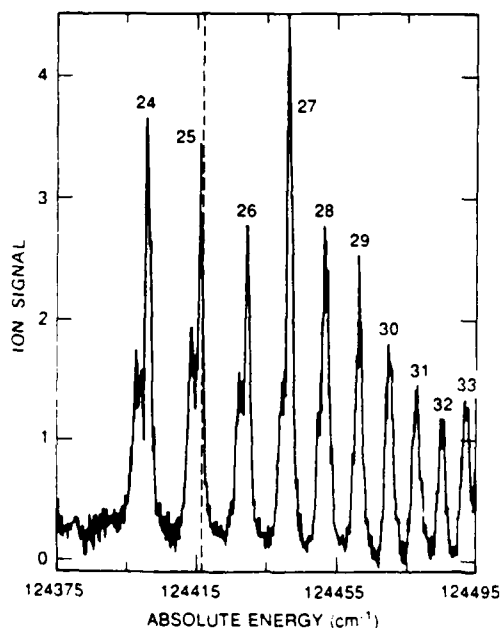


FIG. 2. A plot of the ion signal (arbitrary units) as the second dye laser wavelength is scanned to excite the $J=2 E, F$ ($v=0$) state to the np Rydberg series in the vicinity of $\text{H}_2^+(N=0)$ threshold. The position of the threshold at zero field is indicated by the broken line.

the same N are nearly degenerate. There is a single $J=1$ np Rydberg series converging to the lowest $N=0$ rotational state of vibrationless H_2^+ . Similarly, there are three nearly degenerate np Rydberg series, $J=1, 2,$ and $3,$ converging to the first excited $N=2$ rotational state of H_2^+ . Including the $J=3$ series converging to the $N=4$ state of H_2^+ , there are five Rydberg series that can be excited by the second dye laser photon from the $J'=2 E, F$ state. Owing to the required change in core rotational quantum number, the $J=1$ series converging to the $n=0$ limit and the $J=3$ series converging to the $N=4$ limit have small excitation probability. However, those np states ($J=1, 2,$ and 3) which converge to $\text{H}_2^+(N=2)$ limit and lie above the $\text{H}_2^+(N=0)$ limit, can be excited with good transition probability and they can rotationally autoionize by the process $\text{H}_2(np, J) \rightarrow \text{H}_2^+(N=0) + e(\epsilon)$ where ϵ is the kinetic energy of the ejected electron. Rotational autoionization in H_2 was first observed by Herzberg and Jungen⁷ and later by Dehmer and Chupka.⁹

Now consider a molecule in an electric field F , which is applied along the z axis. The Coulomb potential experienced by the Rydberg electron in an external field is $V = -1/r - zF$ (in atomic units).¹³ Since the saddle point in the combined potential occurs at a distance of $z = F^{-1/2}$, the potential at the saddle point is $-2F^{1/2}$. Viewed classically, ionization occurs if the electron energy W is at or above the saddle-point potential. Thus, in the presence of the electric field the ionization potential is lowered by $-2F^{1/2}$.¹⁴ Therefore, those np Rydberg states converging to the $\text{H}_2^+(N=2)$ limit which lie at energies between I and $I - 2F^{1/2}$ [where I is the $\text{H}_2^+(N=0)$ ionization limit] are able to rotationally autoionize because the continuum channel is opened by the electric field for these states. This process is held responsible for the appearance of the $n=24$ and $n=25$ members in Fig. 2.

The most straightforward way to test the prediction of the classical model outlined above is to observe the spectra in the absence of dc field and confirm the disappearance of the $n=24p$ and $25p$ states. Our detection scheme, however, requires a minimum nominal field of about 15 V/cm as explained above. In order to check the prediction of the classical model, we note the following additional observations. First, note that as shown in Fig. 2, the $n=24p$ and $25p$ states appear when an electric field of only 15 V/cm is applied. This is consistent with our model, since these states require fields of 0.15 and 2.5 V/cm , respectively, for forced autoionization. It is worth noting that at fields of 15 V/cm , we do not observe the ion signal emanating from the excitation of the $n \leq 23p$ states. According to the classical model, the $n=23p$ state which lies 30 cm^{-1} below the $\text{H}_2^+(N=0)$ limit should ionize at a field of 30 V/cm . In Fig. 3 we show the appearance of the $23p$ ionization signal as the dc field is increased, while the second dye laser wavelength is kept fixed at the $E, F \rightarrow 23p$ transition wavelength. From Fig. 3, it is evident that the threshold field for rotational autoionization is $\sim 30 \text{ V/cm}$, in agreement with that obtained from the model outlined above. Similarly, we have observed the onset of rotational autoionization of the $22p$ state, and the observed threshold field (90 V/cm) agrees well with the classical model. We note that the forced rotational autoionization of the $25p$

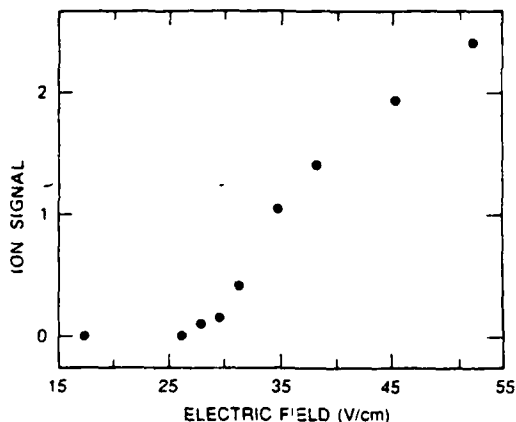


FIG. 3. A plot of the forced-rotational autoionization signal (arbitrary units) of the $23p$ ($J=1, 2, 3$) state converging to the $H_2^+(N+2)$ limit as a function of the electric field.

state converging to the $H_2^+(N=2)$ limit was the first observed by Dehmer and Chupka⁹ in their experiment at a constant electric field of 10 V/cm. Recently, Knight, Zhu, and Wang¹¹ observed the forced rotational autoionization of the triplet $25d$ state.

We have also observed the $J=1$ np Rydberg states when excited from the $J'=0$ E, F state. In this case, the dipole selection rules allow the excitation of a single $J=1$ np series converging to $H_2^+(N=2)$ limit, $np2$, and the $J=1$ np series converging to the $H_2^+(N=0)$ limit, $np0$. The ion spectrum from the $J=1$ np series excited in a 15 V/cm field is shown in Fig. 4.

In Fig. 4, the $J=1$ np resonances converging to $H_2^+(N=2)$ limit appear as windows^{7,9} in the continuum of the $J=1$ series converging to the $H_2^+(N=0)$. These windows, which are quite symmetric, appear because laser excitation from the $J'=0$ state favors those electronic states that have primarily the $N=0$ H_2^+ ion core character. Thus, laser excitation, at energies greater than the $H_2^+(N=0)$ limit, favors primarily the $H_2^+(N=0) + e(l=1)$ open channel. In the vicinity of the $np2$ state converging to the $H_2^+(N=2)$ limit, the effective phase of the $N=0$ open channel undergoes a phase change of π ,¹⁵ and the effective transition moment goes to zero. The resonances in the ion signal shown in Fig. 4 do not reach zero value due to the finite bandwidth of the second laser and due to several continua that may be open due to the electric field. The symmetric window resonances indicate that the Fano- q -factor¹⁵ (which is the ratio of the discrete excitation versus the continuum excitation) is nearly zero. The appearance of windows for the $n=24p$ and $25p$ states along with $n > 26p$ states is evident from Fig. 4. The resonances shown in Fig. 4 are at the same position as those shown in Fig. 2, except that the resonances shown in Fig. 4 represent a single $J=1$ state, while those shown in Fig. 2 are due to the nearly degenerate $J=1, 2,$ and 3 np states.

In examining the ion spectra of np Rydberg states

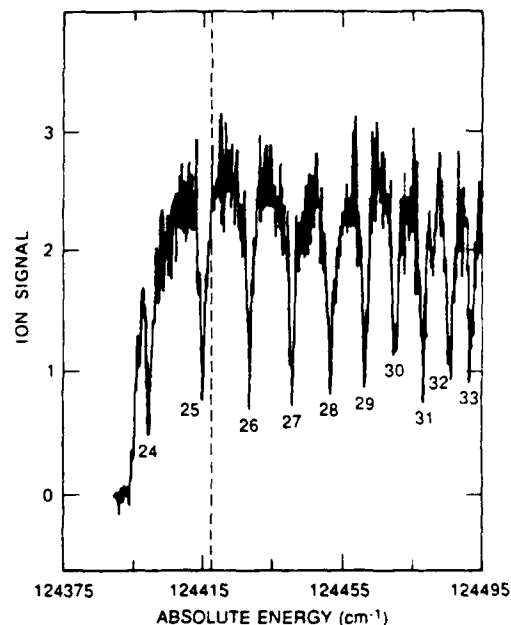


FIG. 4. A plot of the ion signal (arbitrary units) as the second dye laser wavelength is scanned to excite the $J=0$ E, F ($v=0$) state to the $J=1$ np Rydberg series in the vicinity of $H_2^+(N=0)$ threshold, which is shown as the broken line.

shown in Fig. 2, in detail, it is clear that the peaks appear to be split into two or possible three states. From the laser excitation scheme, we expect that the $J=1, 2,$ and 3 components converging to the $H_2^+(N=2)$ limit can be excited from $J'=2$ the E, F state. Based on parity considerations, it is possible for $J=1$ and $J=3$ states converging to the $H_2^+(N=2)$ limit to autoionize with the ejection of an electron with $l=1$ (p wave) and $l=3$ (f wave), respectively. However, in the absence of an external electric field no such open channel exists for the $J=2$ states. As a result, we expect that in the absence of an electric field, at most, two $np2$ resonances converging to the $H_2^+(N=2)$ limit will exist.

There is an additional possibility for producing the split structure in the Rydberg series excited from $J=2$ of the E, F state. The electric field mixes the ep and ed continua and J is no longer a good quantum number. A rough calculation indicates that if a quantum defect of 0.2 is assumed for the p state, then at a field of 15 V/cm at $n=26$ it has 5% d character mixed into it, thus allowing the autoionization of the $J=2$ state. A more detailed analysis of the split structure of the resonances in Fig. 2 is currently being carried out.

Useful discussions with Dr. David L. Huestis and Dr. James R. Peterson are gratefully acknowledged. This research was supported by the U.S. Air Force Office of Scientific Research under Contract No. F49620-86-K-0017.

- ¹W. R. S. Garton and K. Codling, *Proc. Phys. Soc. London* **75**, 87 (1960).
- ²C. M. Brown and M. L. Ginter, *J. Opt. Soc. Am.* **68**, 817 (1978).
- ³W. E. Cooke and T. F. Gallagher, *Phys. Rev. Lett.* **41**, 1648 (1978).
- ⁴J. A. Armstrong, P. Esherick, and J. J. Wynn, *Phys. Rev. A* **15**, 180 (1970).
- ⁵E. E. Eyler, *Phys. Rev. A* **34**, 2881 (1986).
- ⁶U. Fano, *Phys. Rev. A* **2**, 353 (1970).
- ⁷G. Herzberg and Ch. Jungen, *J. Mol. Spectrosc.* **41**, 425 (1972).
- ⁸W. R. S. Garton, W. H. Parkinson, and E. M. Reeves, *Proc. Soc. London* **80**, 860 (1962).
- ⁹P. M. Dehmer and W. A. Chupka, *J. Chem. Phys.* **65**, 2243 (1976).
- ¹⁰G. R. Janik, O. C. Mullins, C. R. Mahon, and T. F. Gallagher, *Phys. Rev. A* **35**, 2345 (1987).
- ¹¹R. D. Knight, J. E. Sohl, Y. Zhu, and L.-G. Wang, in *Proceedings of the Conference on Laser Spectroscopy VIII, Are, Sweden, 1987*, Springer Series in Optical Sciences, Vol. 55, edited by W. Persson and S. Svanberg (Springer-Verlag, New York, 1987), p. 198.
- ¹²E. E. Marinero, C. T. Rettner, and R. N. Zare, *Phys. Rev. Lett.* **48**, 1323 (1982).
- ¹³M. G. Littman, M. M. Kash, and D. Kleppner, *Phys. Rev. Lett.* **41**, 103 (1978).
- ¹⁴E. Y. Xu, H. Helm, and R. Kachru, *Phys. Rev. Lett.* **59**, 1096 (1987).
- ¹⁵U. Fano, *Phys. Rev.* **124**, 1866 (1961).

Appendix D

FIELD IONIZATION OF HIGH-LYING STATES OF H₂

Field Ionization of High-Lying States of H_2

E. Y. Xu, H. Helm, and R. Kachru

Chemical Physics Laboratory, SRI International, Menlo Park, California 94025

(Received 26 June 1987)

We report the first systematic study of the field ionization threshold of molecular Rydberg states. We find that the $v=0$ np series of both orthohydrogen and parahydrogen, converging to the lowest rotational state of H_2^+ , with n ranging from 18 to 30, ionize at fields given by $1/16n^4$, with n_s , the effective quantum number at the field at which ionization takes place, given by $n_s = n - 0.5$. Our threshold-field measurements suggest that the ionization process is described classically.

PACS numbers: 33.55.Be, 34.60.+z

The ionization by means of an external electric field of excited atoms has long attracted considerable experimental¹⁻⁷ and theoretical⁸ interest. The field-induced ionization process in atoms is now a fairly well understood and a practically useful phenomenon. In some cases, such as in atomic hydrogen,⁶⁻⁸ ionization occurs by tunneling of the electron through the potential barrier along the axis of the applied external field. In other cases, such as nonhydrogenic atomic states with finite quantum defects, the field ionization is described by a classical "saddle-point" model,² in which states are stable or unstable against ionization if they are below or above the saddle point in the combined Coulomb and external potential. Apart from its scientific interest, field ionization (FI) has important applications, such as selective detection with high sensitivity in experiments involving excited species.

It has long been known that the molecular Rydberg states are field ionizable,⁹⁻¹¹ and this phenomena has been employed in many experiments for the detection of the excited molecules. However, apart from the n^{-4} scaling of the ionization field,⁹ where n is the principle quantum number, nothing else is known about the ionization mechanism. It is not known if these molecules ionize like a hydrogenic atom or like an alkali-metal atom. Also, it is not known to what extent the core rotation plays any role in the ionization process.

In this Letter we report for the first time the study of the onset of ionization of H_2 molecules in a single quantum state, when a quasistatic electric field is applied. We find that the $v=0$ np states of H_2 , with n ranging from 18 to 30, and converging to the $N=0$ and 1 rotational states of the vibrationless H_2^+ core, ionize at fields close to the $1/16n^4$ classical limit. Furthermore, we find that for the Rydberg states studied thus far, the field ionization thresholds for states of different total angular momentum J (disregarding the spin), but same N , are the same, which suggests that the electron-core rotational interaction plays no part in the ionization process.

The experimental arrangement consists of a pulsed H_2 supersonic beam, which is turned on for 100 μ s. The H_2 beam passes between two field plates, spaced 1 cm apart. One of the plates has a 7-mm-diam hole with a grid for

ion extraction. The pulsed nozzle, the plates, and the detector are all housed in a vacuum chamber pumped to 3×10^{-8} Torr. When the H_2 beam is turned on, the pressure rises to 5×10^{-5} Torr and provides a high H_2 -number density in the interaction region in a collision-free environment. The H_2 beam is intersected near the center of the plates by two counterpropagating tunable dye laser beams which are focused by a 10-cm-focal-length lens. The first dye laser beam, with $\lambda_1 = 200$ -201 nm, is produced by our, first, frequency doubling the output of an yttrium-aluminum-garnet-pumped dye laser, and then Raman shifting the frequency-doubled output to the fourth anti-Stokes order in a high-pressure H_2 cell. The first dye laser with a typical energy of 100 μ J/pulse and a spectral width of 1 cm^{-1} , excites the H_2 molecules by a two-photon process from the initial $v''=0, J''=0$ (1) $X^1\Sigma_g^+$ ground state to the $v'=0, J'=0$ (1) $^1\Sigma_g^+$ E - F excited state. The second dye laser, with $\lambda_2 = 398$ -403 nm, spectral linewidth of 0.5 cm^{-1} , and energy of 500 μ J/pulse, subsequently excites the molecules from the selected E - F state to a $v=0, J=0$ ($J=0, 1$, and 2), np Rydberg state converging to the $N=0$ (1) rotational state of the H_2^+ ion core. The second dye laser is delayed in time with respect to the first one by 30 ns.

A high-voltage pulse of 0.3- μ s rise time and up to 4-kV/cm field amplitude is applied on the extraction plates 0.5 μ s after the laser pulses, field ionizing the Rydberg molecules and accelerating the H_2^+ ions formed into an electron multiplier. Since the FI pulse peaks and remains constant to about 5% of its value for about 0.2 μ s before decaying rapidly, we are in fact measuring ionization rates that are in excess of $10^7 s^{-1}$. The energy levels of the Rydberg series are first mapped out by our scanning the second laser wavelength while keeping the first dye laser fixed on a particular two-photon resonance from the ground state to the E - F state and setting the high-voltage pulse on the field plates to a value high enough to ensure complete ionization of states with $n > 18$.

The plot of the ion signal as a function of the second dye-laser wavelength is used to identify the np $J=0, 1$,

and 2 states. From the measured level positions and previous work by Herzberg and Jungen¹² and by Dieke,¹³ we find that starting from the $J'=1$, ortho ($J'=0$, para) $E-F$ state, we excite primarily the $J=1$ and 2 ($J=1$) np states, converging to the $N=1$ ($N=0$) limit of the H_2^+ ion. The excitation to the other allowed states is weak.

After the Rydberg states are identified, the two dye lasers are tuned to excite the H_2 molecule into an excited np state with a well-defined J and rotational quantum number of the ion core, N . The ionization probability as a function of the applied electric field is studied by our increasing the amplitude of the FI pulse from a small value until an observable threshold is detected. Figure 1 illustrates a typical dependence of the ionization signal as a function of the applied electric field. The abrupt onset of the field ionization is evident in Fig. 1, which shows that beyond the threshold the ionization signal increases rapidly. In Fig. 1, the bump in the ion signal near 500 V/cm is not reproducible, and is due to the signal being noisy. Furthermore, because of the noise in our signal we cannot rule out additional field ionization thresholds at higher fields.

Figure 2(a) shows the measured dependence of the ionization threshold field F_T as a function of the effective principal quantum number n_s , for the ortho- H_2 $J=1$ and 2 Rydberg states converging to the $N=1$ rotational state of H_2^+ . $n_s = n - 0.5$ is the effective quantum defect of the np states, at the field at which ionization takes place. The error bars in Fig. 2 represent the uncertainty in our threshold measurement which is primarily due to the relatively low ion-collection efficiency of our setup. The threshold measurements for the np states that are missing in the plot shown in Fig. 2 were not measured because the excitation probability to these states from the $E-F$ state is small as a result of perturbations from low- n

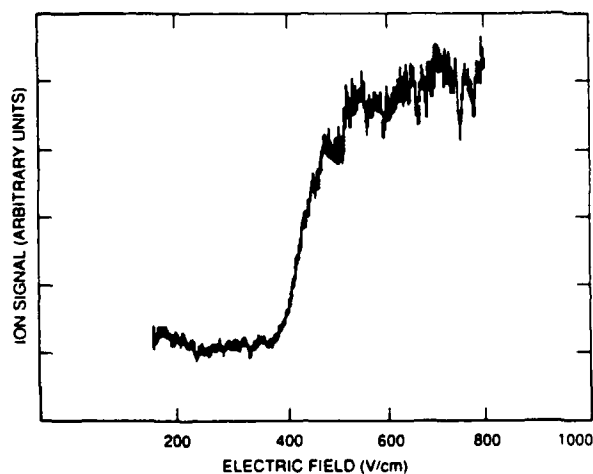


FIG. 1. Field-ionized ion signal as a function of the amplitude of the ionization pulse for $n=30$, p state converging to the $N=1$ rotation state of H_2^+ .

states converging to high vibrational states of H_2^+ . The observed threshold agrees very well with the $1/16n_s^4$ field value, shown as a solid line in Fig. 2, implying that the ionization process is described classically (see discussion below).

The Coulombic potential experienced by the Rydberg electron in an external field is $V = -1/r - Fz$ (in atomic units), where F is the external electric field applied along the z axis. Since the saddle point in the combined potential occurs at a distance $z_s = F^{-1/2}$, the potential at the saddle point is given by $-2F^{1/2}$. Viewed classically, ionization occurs if the electron energy $W = -1/2n^{*2}$ is at or above the saddle-point potential. Note that $n^* = n - \delta$ is the effective quantum number, and δ is the quantum defect. Thus, classically, ionization occurs at $F_T = 1/16n^{*4}$, if the Stark shifts of the energy levels can be

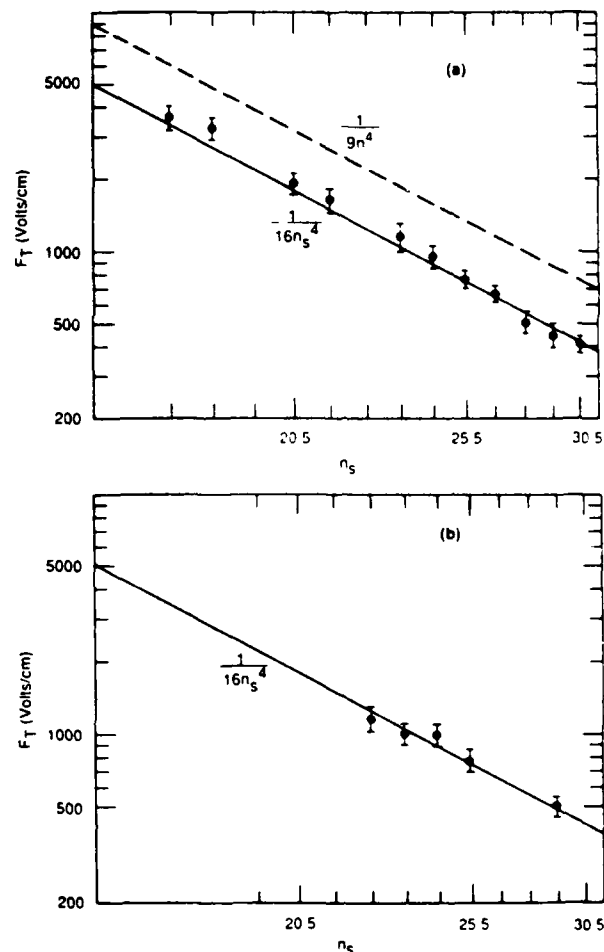


FIG. 2. Threshold field vs n_s ($=n-0.5$) for (a) ortho- H_2 np states converging to the $N=1$ rotational state of H_2^+ , and (b) para- H_2 np states converging to the $N=0$ state of H_2^+ . The solid line is a plot of $F_T = 1/16n_s^4$ and the dashed line is a plot of $F_T = 1/9n_s^4$.

neglected. In the H atom, because of the near perfect Coulomb symmetry, Stark levels from adjacent n manifolds cross each other as the electric field is increased. The red Stark states are on the same side as the saddle point, and the energy of the reddest Stark state of the n manifold is given to a good approximation by $W = -1/2n^2 - \frac{1}{2}n^2F + O(F^2)$. Thus the classical ionization field for the reddest member of the hydrogenic Stark manifold is given by $F_T = 1/9n^4$ and is plotted as a dashed line in Fig. 2(a). It is evident from Fig. 2(a) that the observed field-ionization data for the np states do not fit the $1/9n^4$ value.

For alkali-metal atoms and the H_2 np states, because of the non-Coulombic potential experienced by the electron in the region close to the core, the Coulomb symmetry is broken and, as a result, the states of a given n manifold are mixed with states of adjacent manifolds.² The state mixing due to the non-Coulombic potential is best illustrated with reference to a schematic Stark diagram, shown in Fig. 3. A schematic sketch of the Stark map is drawn because the quantum defects of most of the Rydberg series are unknown. We have assumed a quantum defect of 0.2 for the p state and a zero quantum defect for the higher l states, to illustrate the Stark map more clearly. This assumption does not affect the generality of

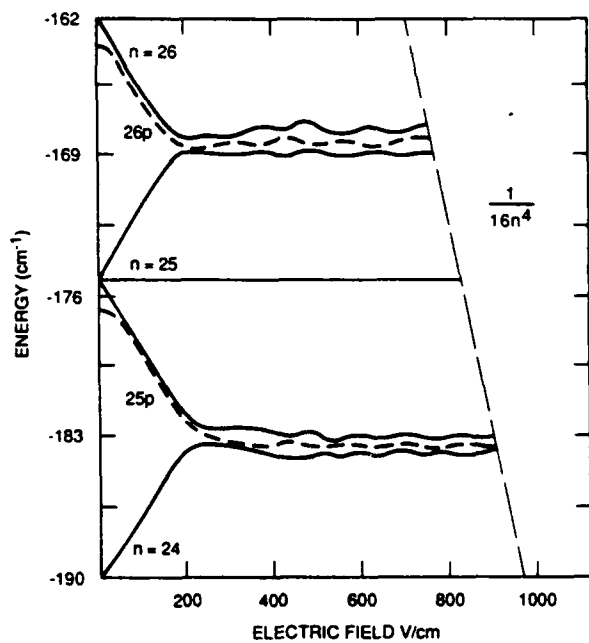


FIG. 3. Schematic of the $|m| = 1$ energy levels in the presence of electric field near $n = 25$. The solid and dashed lines show the approximate adiabatic paths for the ionization of states in the vicinity of $n = 25$. The classical ionization occurs at field values where Stark states intersect with the nearly vertical line representing the energy $W = 1/16n^4$.

1098

the discussion below, because in the $|m| = 1$ Stark-state map, the p state has the largest quantum defect. Figure 3 shows the reddest, bluest, and the central, $|m| = 1$ Stark states of the $n = 24, 25,$ and 26 manifold. In the discussion that follows we neglect, for simplicity, any interaction between states converging to different rotational states of H_2^+ , and we also neglect the electron-core rotational interaction.

At moderate electric fields, the Stark effect becomes linear, until at fields of $1/3n^5$ the red members of the $n = 26$ manifold approach the blue members of the $n = 25$ manifold. The admixture of the $n = 25$ character in the red states of the $n = 26$ manifold, and vice versa, leads to avoided crossings between the states of the two manifolds. At fields greater than $1/3n^5$, there is no change in the energy of the reddest $n = 26$ Stark state and the bluest $n = 25$ state because of the repeated avoided crossings. The binding energy of the reddest $n = 26$ state and the bluest $n = 25$ state at the ionization field is thus approximately represented by an effective quantum number of 25.5. Since the np states are the reddest members of the $|m| = 1$ manifold, it is reasonable to expect that for these, and other nearby states, the field ionization threshold, if adiabatic, is given by $1/16n_s^4$, where $n_s = n - 0.5$. In Fig. 2, the $1/16n_s^4$ threshold field is shown as a solid line. It is evident from Fig. 2(a) that the agreement between the experimentally determined threshold field and that determined from $1/16n_s^4$ is good, except for $n = 19$, which has a somewhat larger field ionization threshold possibly due to perturbations from low- n members of high- v states.¹² The $1/16n_s^4$ threshold field observed for H_2 is similar to that observed for the low- l Na states.⁵

From the above discussion it is clear that for the slow rates that we have used in our experiment, the passage of the electron from the intermediate to the high fields is substantially adiabatic. For, if it were not so, we would have observed ionization thresholds near $1/9n^4$ which is far in excess of the observed values.

We have also studied the ionization threshold of the $J = 1$ np series converging to the $N = 0$ state of H_2^+ , and these data are shown plotted as a function of n , in Fig. 2(b). The ionization thresholds for the states of this series are the same as they are for the states converging to the $N = 1$ limit. However, there is more scatter in the data for the series converging to the $N = 0$ limit because of the overall lower signal. The n dependence of the ionization threshold as shown in Fig. 2(b) agrees quite well with the $1/16n_s^4$ scaling, with $n_s = 0.5$, and is shown as a solid line in the figure.

For the np Rydberg series converging to the $N = 1$ limit, we have made measurements of the ionization thresholds of states with the same N but different J values ($J = 1$ and 2) arising from the $J = N + l$ coupling of the electron orbital angular momentum and the core rotational angular momentum. We find no discernible difference in the ionization threshold of these states with different J . No measurements of the $J = 0$ np states were

made because the excitation to these states from the $J'=1$ E - F states is small. In addition, the 0.5-cm^{-1} linewidth of the second laser allows us to distinguish the $J=1$ and 2 states for $n < 27$. However, for $n > 27$, the observed ion signal represents field ionization from a mixture of $J=1$ and 2 states. Since we find no discernible difference in the ionization threshold for the np $J=1$ and 2 states below $n=27$, it is reasonable to expect the same for states with $n > 27$. This result means that for the states we have studied, the core rotation does not play a significant part in the dynamics of the field ionization.

Useful discussions with Dr. David L. Huestis are gratefully acknowledged. This research was supported by the U.S. Air Force Office of Scientific Research under Contract No. F49620-86-K-0017.

¹Theodore W. Ducas, Michael G. Littman, Richard R. Freeman, and Daniel Kleppner, Phys. Rev. Lett. **35**, 366 (1975).

²Michael G. Littman, Michael M. Kash, and Daniel

Kleppner, Phys. Rev. Lett. **41**, 103 (1978).

³R. F. Stebbings, C. J. Lattimer, W. P. West, F. P. Dunning, and T. B. Cooke, Phys. Rev. A **12**, 1453 (1975).

⁴Myron L. Zimmerman, Michael G. Littman, Michael M. Kash, and Daniel Kleppner, Phys. Rev. A **20**, 2251 (1979).

⁵T. F. Gallagher, L. M. Humphrey, W. E. Cooke, R. M. Hill, and S. A. Edelstein, Phys. Rev. A **16**, 1098 (1977).

⁶J. E. Bayfield and P. M. Koch, Phys. Rev. Lett. **33**, 258 (1974).

⁷P. M. Koch and D. R. Mariani, Phys. Rev. Lett. **46**, 1275 (1981).

⁸D. S. Bailey, J. R. Hiskes, and A. C. Riviere, Nucl. Fusion **5**, 41 (1965).

⁹C. F. Barnett, J. A. Ray, and A. Russek, Phys. Rev. A **5**, 2110 (1972).

¹⁰T. J. Morgan, C. F. Barnett, J. A. Ray, and A. Russek, Phys. Rev. A **20**, 1062 (1979).

¹¹Ravinder Kachru and Hanspeter Helm, Phys. Rev. Lett. **55**, 1575 (1985).

¹²G. Herzberg and C. H. Jungen, J. Mol. Spectrosc. **41**, 425 (1972).

¹³*The Hydrogen Molecule Wavelength Tables of Gerhard Heinrich Dieke*, edited by H. M. Crosswhite (Wiley-Interscience, New York, 1972).